

Out-of-equilibrium relaxation of the Edwards-Wilkinson elastic line

Sebastian Bustingorry¹, Leticia F. Cugliandolo² and José Luis Iguain³

¹DPMC-MaNEP, Université de Genève, 24 Quai Ernest Ansermet, 1211 Genève 4, Switzerland

²Université Pierre et Marie Curie – Paris VI, LPTHE UMR 7589, 4 Place Jussieu, 75252 Paris Cedex 05, France

Departamento de Física, FCEyN, Universidad Nacional de Mar del Plata
Deán Funes 3350, 7600 Mar del Plata, Argentina

Abstract. We study the non-equilibrium relaxation of an elastic line described by the Edwards-Wilkinson equation. Although this model is the simplest representation of interface dynamics, we highlight that many (not though all) important aspects of the non-equilibrium relaxation of elastic manifolds are already present in such quadratic and clean systems. We analyze in detail the aging behaviour of several two-times averaged and fluctuating observables taking into account finite-size effects and the crossover to the stationary and equilibrium regimes. We start by investigating the structure factor and extracting from its decay a growing correlation length. We present the full two-times and size dependence of the interface roughness and we generalize the Family-Vicsek scaling form to non-equilibrium situations. We compute the incoherent scattering function and we compare it to the one measured in other glassy systems. We analyse the response functions, the violation of the fluctuation-dissipation theorem in the aging regime, and its crossover to the equilibrium relation in the stationary regime. Finally, we study the out-of-equilibrium fluctuations of the previously studied two-times functions and we characterize the scaling properties of their probability distribution functions. Our results allow us to obtain new insights into other glassy problems such as the aging behavior in colloidal glasses and vortex glasses.

Keywords: Slow dynamics and aging (theory), self-affine roughness (theory), kinetic growth processes (theory)

1. Introduction

1.1. Aim

Interfaces are important in many physical, chemical and biological phenomena. In the physical context they appear in stochastic surface growth [1], domain growth and coarsening phenomena (as domain walls) [2], type-II superconductivity (as magnetic flux lines) [3], fracture cracks [4], and fluid invasion in porous media [5], among others realizations. Although specific problems involve different levels of complexity, as the inclusion of non-linear or disorder contributions, the main features of interface dynamics are already contained in the simplest theoretical formulation of the problem: the Edwards-Wilkinson (EW) equation [6].

The aim of this article is to exhibit, in a concrete and fully solvable example, several generic properties of the averaged and fluctuating aging dynamics of finite and infinite elastic manifolds. The problem we analyze is the relaxation of an elastic line described by the Edwards-Wilkinson equation [6]. The embedding space dimension plays an important role. In the particular one dimensional transverse space case on which we focus here the dynamics has aspects of diffusion, glassiness and saturation depending on the time and length scales observed.

The relaxation process we are interested in is the following [7]. After equilibration at a temperature T_0 the system is suddenly taken to a different working temperature T that can be higher or lower than T_0 . Time is then set to zero. The line subsequently tries to adapt to the working temperature. The relaxation is characterized by the time-dependence of correlation and linear response functions. One lets the line relax until a waiting-time, t_w , when the quantities of interest are first recorded and later compared to their values at a subsequent time t .

A series of glassy properties of elastic lines evolving in disordered environments have been recently reported in different contexts, related to directed polymers in random media [8, 9], the vortex glass dynamics in high temperature superconductors [10, 11, 12], and domain wall motion in magnetic systems [13, 14]. All these studies focused on models including disorder, which non-disordered counterparts belong to the EW universality class of interface dynamics [1], except for Ref. [14] in which the analysis is focused on the non-linear contribution in the Kardar-Parisi-Zhang (KPZ) [15] universality class. In order to disentangle the effects of elasticity and disorder it is then important to study in detail the dynamics of the non-disordered counterparts.

In general, the glassy phenomenon in finite dimensional models of elastic lines with and without quenched disorder appears as a dynamic crossover [8, 9, 10]. For all waiting-times, t_w , that are longer than a size, L , and eventually also temperature, T , dependent *equilibration time*, t_L , the dynamics is stationary. Instead, for $t_w < t_L$ the system is in the preasymptotic regime and the relaxation occurs out of equilibrium as demonstrated by two-times correlations and linear responses that age. For each waiting-time the dependence on the time-delay, $\Delta t \equiv t - t_w$, then shows a growth regime for $\Delta t < t_L$ and saturation regime at longer time, $\Delta t > t_L$, where the correlation functions saturate

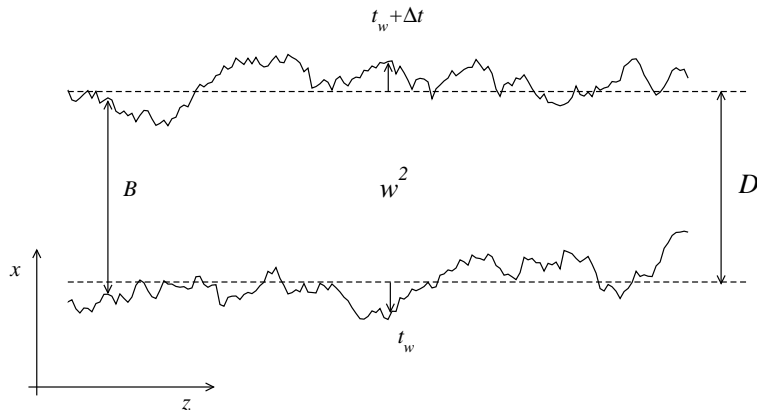


Figure 1. Two line configurations at different times, e.g. $x(z, t_w)$ and $x(z, t_w + \Delta t)$, showing the relevant displacements defining the mean-squared-displacement of the line segments, B , the roughness, w^2 , and the mean-squared-displacement of the center of mass, D .

to a size dependent value.

Here we compute, analytically, the averaged two-times roughness and we relate it to the displacement field, which was the main focus of previous studies of the dynamics of elastic manifolds in random environments [8, 10, 16], and the center of mass evolution of the interface (see the sketch in Fig. 1). The quadratic character of the model allows us to control the crossover to equilibration and saturation of finite lines. We next deduce several other correlators that are of interest in glassy dynamics. In particular, we analyze the incoherent scattering function and compare it to light scattering measurements in clay colloidal suspensions [17]. We interpret our results in terms of a two-times correlation length that we evaluate and confront to the one measured in other aging glassy systems [18, 19]. We also study linear responses and their relation to the companion correlations. We discuss in detail the special features of these two-times observables linked to the multiplicative – diffusive – scaling form.

Finally, we focus on thermally induced fluctuations. Recently, the importance of studying fluctuations – and not only averaged quantities – in dynamic phenomena was stressed in several contexts. Rácz proposed to use scaling functions characterizing the fluctuations of global observables in *non-equilibrium steady states* to classify systems in ‘universality classes’ dictated by symmetries and dynamic mechanisms [20]. In *aging glassy* systems the study of fluctuations seems to be fundamental to understand the mechanism for the dramatic slowing down and non-equilibrium relaxation. Chamon *et al* [21, 22] proposed a symmetry based sigma-model like theory for fluctuations in conventional glassy systems. For a number of reasons this theory is not expected to apply, without modification, to interface dynamics. In more technical terms, the averaged interface dynamics is characterized by a multiplicative aging scaling that should result in the need to modify the approach in [21] to take this feature into account. We thus wish to confront the fluctuations of conventional glassy systems to those of interface models searching for similarities and differences. With this purpose we derive

the probability density functions (pdfs) of several two-times correlation functions. We compare our results to previous studies [23], which focused on the time-delay dependence of the fluctuations ‡, and to predictions of the time-reparametrization invariance scenario of glassy systems [21, 22].

The problem addressed here is related to a number of other models that have already been studied in the literature; among the pure cases one has the Langevin dynamics of the Gaussian and massless scalar field [24], the XY ferromagnet [24, 25], the $p = 2$ spherical spin-glass [26] and the $O(N)$ ferromagnet in the large N limit [27]. Related models with quenched disorder are problems of elastic manifolds in quenched random environments [8, 9, 13, 16]. In all these studies the finite size dependence was not taken into account and the dynamic fluctuations were not studied. We explain in the conclusions how our results relate to the ones in these papers.

1.2. The model

The EW equation for a scalar field x representing the height of a surface over a one dimensional substrate parametrized by the coordinate z (a one dimensional directed interface) is

$$\partial_t x(z, t) = \nu \partial_z^2 x(z, t) + f(z, t) + \xi(z, t), \quad (1)$$

$$\langle \xi(z, t) \rangle = 0, \quad \langle \xi(z, t) \xi(z', t') \rangle = \frac{2T}{\gamma} \delta(z - z') \delta(t - t'), \quad (2)$$

with $\nu = c/\gamma$, c the elastic constant, γ the friction coefficient, T the temperature of the thermal bath and $\langle \dots \rangle$ the average over the white noise ξ , *i.e.* the thermal average. The term $f = h/\gamma$ represents the effect of a perturbing field that couples linearly and locally to the height, $-h(z, t)x(z, t)$. One can also consider other types of perturbations that couple to more complicated functions of the height, as discussed in Sect. 7.

We are interested in characterizing the dynamics of elastic lines with *finite* and *infinite* length L . Thus for convenience we shall take periodic boundary conditions in the z -direction. Following Antal and Rácz we introduce a Fourier representation of the position dependent distance of the line from its average [23]

$$\delta x(z, t) \equiv x(z, t) - \bar{x}(t) = \sum_{n=-\infty}^{\infty} c_n(t) e^{ik_n z}, \quad (3)$$

with $k_n = 2\pi n/L$. The overline indicates an average over the full line's configuration;

$$\bar{x}(t) = \frac{1}{L} \int_0^L dz x(z, t) \quad (4)$$

being then the mean height – or center of mass – of the interface. The Fourier coefficients are given by

$$c_n(t) = \frac{1}{L} \int_0^L dz [x(z, t) - \bar{x}(t)] e^{-ik_n z} \quad (5)$$

‡ We note that the solution presented in [23] corresponds actually to the $t_w = 0$ solution in this article.

and their evolution is given by

$$\partial_t c_n(t) = -\nu k_n^2 c_n(t) + f_n(t) + \xi_n(t), \quad (6)$$

$$\langle \xi_n(t) \rangle = 0, \quad \langle \xi_n(t) \xi_{n'}(t') \rangle = \frac{2T}{\gamma L} \delta_{n,-n'} \delta(t-t') \quad (7)$$

for all $n \neq 0$ while $c_0(t) = 0$ at all t . Note that equation (6) effectively describes the position of a particle in a harmonic potential with spring constant νk_n^2 which implies an elastic constant softening with decreasing n or increasing system size L . The solution to equation (6) is

$$c_n(t) = c_n(0) e^{-\nu k_n^2 t} + e^{-\nu k_n^2 t} \int_0^t dt' e^{\nu k_n^2 t'} [\xi_n(t') + f_n(t')]. \quad (8)$$

where we set the initial time to $t = 0$. The coefficients $c_n(0)$ encode the structure of the initial conditions. We are interested in the evolution after an instantaneous quench from equilibrium at a generic temperature T_0 to the working temperature T . We are then considering that the initial conditions satisfy

$$\langle c_n(0) c_m(0) \rangle_{ic} = |c_n(0)|^2 \delta_{n,-m}, \quad (9)$$

where $|c_n(0)|^2$ should reflect the equilibrium at T_0 (see below). When the initial temperature is higher than the working temperature, $T_0 > T$, the initial state is more disordered than the equilibrium one at T and the line tends to ‘order’ as time elapses. On the other hand, when $T_0 < T$, temperature fluctuations roughen the initial – more ordered – configuration of the line. A special case is $T_0 = 0$, corresponding to a perfectly flat initial configuration.

The EW energy is just the one of a massless scalar field and the model does not have a finite temperature static phase transition.

Through out the article we shall present some figures which highlight the main analytical results. Without loss of generality we set $\gamma = \nu = 1$ in all the figures. We distinguish noise averaged from fluctuating quantities by enclosing the former with angular brackets. In our expressions we do not write explicitly the T , T_0 and L dependencies but one has to keep in mind that they are, in principle, always present.

1.3. Organization of the paper

The organization of the paper is the following. In Sect. 1.2 we had introduced the model and our conventions. Section 2 deals with the two-times structure factor and Sect. 3 with the associated two-times correlation length. In Sect. 4 we analyze the line’s roughness and in Sect. 5 we study the displacement field as well as the motion of the center of mass. In Sect. 6 we derive a wave-vector dependent correlation inspired in the incoherent scattering function typical of particles in interaction. Section 7 analyzes different linear response functions and their relation to the associated correlations that is to say the modifications of the fluctuation-dissipation theorem (FDT). In Sect. 8 we study thermally induced fluctuations by computing the probability distribution function of the roughness, displacement and linear responses and we relate to previous studies of

elastic lines in equilibrium as well as with the proposal for fluctuations in aging systems based on the development of time-reparametrization invariance. Finally, in Sect. 9 we summarize our results and we present our conclusions. The main features of the chosen observables are shown in figures that display the *analytic* solution.

2. Two-times structure factor

A key quantity in the two-times evolution of the elastic line is the local displacement of the surface height, defined as $u(z, t, t_w) \equiv x(z, t) - x(z, t_w)$, which allows for the two-times generalization of several quantities. The structure factor associated to this displacement is

$$\begin{aligned} \langle S_n \rangle(t, t_w) &= L \langle |c_n(t) - c_n(t_w)|^2 \rangle \\ &= \frac{T_0}{\gamma \nu k_n^2} \left(1 - e^{-\nu k_n^2 |\Delta t|}\right)^2 e^{-2\nu k_n^2 t_w} \\ &+ \frac{T}{\gamma \nu k_n^2} \left[2 \left(1 - e^{-\nu k_n^2 |\Delta t|}\right) \left(1 - e^{-2\nu k_n^2 t_w}\right) + \left(1 - e^{-2\nu k_n^2 |\Delta t|}\right) e^{-2\nu k_n^2 t_w} \right]. \end{aligned} \quad (10)$$

The structure factor defined in this way is the two-times generalization of the one commonly used in the solution of the EW equation [13, 28]; by definition, it is symmetric under $t \leftrightarrow t_w$. Hereafter we take $t \geq t_w$, dropping the absolute value in the exponentials.

One can easily obtain several limits that show the complexity of the aging behavior. Let first consider the stationary limit, which is reached when $\nu k_n^2 t_w \gg 1$ for all n in (10). This condition is fulfilled when $t_w \gg t_L$, where

$$t_L \equiv \frac{L^2}{4\pi^2 \nu} \quad (11)$$

is a characteristic time marking the onset of finite size equilibration, and which will play an important role in the expressions below. Then, in the stationary limit, the structure factor becomes

$$\lim_{\nu k_n^2 t_w \gg 1} \langle S_n \rangle(t, t_w) = \frac{2T}{\gamma \nu k_n^2} \left(1 - e^{-\nu k_n^2 \Delta t}\right). \quad (12)$$

If one subsequently takes the small wave-vector limit for a given Δt , *i.e.* $\nu k_n^2 \Delta t \ll 1$, the structure factor reaches the generic asymptote $\langle S_n \rangle = 2T\Delta t/\gamma$. On the other hand, if one takes the large wave-vector limit for a given Δt , *i.e.* $\nu k_n^2 \Delta t \gg 1$, one finds the power-law decay of the structure factor

$$\lim_{\substack{\nu k_n^2 t_w \gg 1 \\ \nu k_n^2 \Delta t \gg 1}} \langle S_n \rangle(t, t_w) = \frac{2T}{\gamma \nu k_n^2}, \quad (13)$$

typically found in harmonic processes. Thus, this is the typical stationary solution of the structure factor, displaying the Δt -dependent saturation in the small wave-vector limit and the $1/k_n^2$ behavior in the long wave-vector limit corresponding to the modes already equilibrated at the temperature T [13]. When $\Delta t \gg t_L$ all the modes are equilibrated

at the working temperature and the structure factor shows the power-law behavior in (13) for all k_n , without the saturation regime. This behaviour indicates that the large wave-vectors equilibrate first at the working temperature, and then, for increasing time-delay, the number of equilibrated modes increase. This is obviously related to a growing correlation length, which will be analyzed in Sec. 3, together with its aging behaviour.

Now, let see how the waiting-time dependence modifies the behaviour of the structure factor. First one notices that the small wave-vector saturation asymptote does not depend on the waiting time, *i.e.* the saturation value

$$\lim_{\nu k_n^2 \Delta t \ll 1} \langle S_n \rangle(t, t_w) = \frac{2T}{\gamma} \Delta t, \quad (14)$$

is t_w -independent but time-delay-dependent. On the other hand, the waiting-time is most prominent in the asymptotic power-law regime, $\nu k_n^2 \Delta t \gg 1$, where one finds

$$\lim_{\nu k_n^2 \Delta t \gg 1} \langle S_n \rangle(t, t_w) = \frac{T_0}{\gamma \nu k_n^2} e^{-2\nu k_n^2 t_w} + \frac{T}{\gamma \nu k_n^2} \left(2 - e^{-2\nu k_n^2 t_w} \right). \quad (15)$$

From this expression one observes that the asymptotic power-law regime in the large wave-vector limit changes from the $(T_0 + T)/(\gamma \nu k_n^2)$ asymptote at small waiting-time, to the $2T/(\gamma \nu k_n^2)$ asymptote in the long waiting-time limit. For a fixed time-delay value such that $\Delta t > t_w$, and for modes such that $\nu k_n^2 \Delta t \gg 1$, the power-law behaviour changes from $(T_0 + T)/(\gamma \nu k_n^2)$ at lower values of k_n to $2T/(\gamma \nu k_n^2)$ at higher values, indicating that the large wave-vectors $\nu k_n^2 t_w \gg 1$ are equilibrated at the working temperature, while the other modes still reflect the initial condition. This also implies the existence of a waiting-time-dependent mode, $k_w \sim (\nu t_w)^{-1/2}$, which separates these two regimes, allowing us to write the structure factor, in the asymptotic time-delay limit, in a scaling form:

$$\lim_{\nu k_n^2 \Delta t \gg 1} \langle S_n \rangle(t, t_w) = k_w^{-2} \mathcal{S}(k/k_w). \quad (16)$$

In Figs. 2-4 we display the analytic results explained above. In Fig. 2 we show the $T = 1$ evolution of the structure factor $\langle S_n \rangle$ after heating a perfectly flat initial condition, *i.e.* from $T_0 = 0$. The first panel illustrates the time-delay saturation value and the power-law decay at large k_n , where the change between the two asymptotes, which are proportional to $T_0 + T$ and $2T$, is clear. Figure 2 (b) shows the crossover at $k_w \sim (\nu t_w)^{-1/2}$, between the two asymptotes using different waiting-times and the large time-delay limit $\Delta t \gg t_L$. In this case, *i.e.* $T > T_0$, the equilibrated asymptote, proportional to $2T$, is the upper dashed line. In Fig. 3 (a) we show the dynamics after a quench from $T_0 > T$; the approach to the saturation value at small k_n is non-monotonic. In the asymptotic time-delay limit shown in panel (b), $\langle S_n \rangle$ crosses over from a higher value asymptote at small wave-vector to a lower value at large wave-vector, proportional to $2T$ and corresponding to equilibration, at the waiting-time dependent value k_w in equation (16). In Fig. 4 we study the dependence on the initial condition, T_0 , finding that the height and width of the bump increase with T_0 .

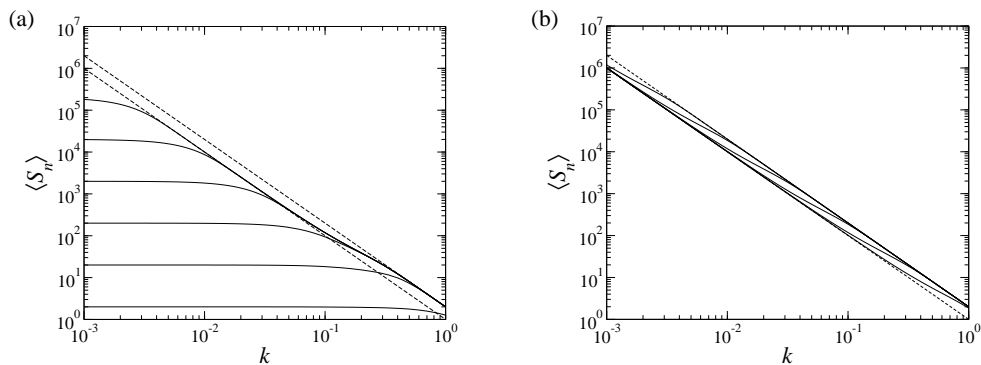


Figure 2. $T = 1$ evolution of the structure factor from a flat initial condition ($T_0 = 0 < T$). (a) $t_w = 10$ and the curves correspond to the time-delay values $\Delta t = 1, 10, 10^2, 10^3, 10^4$, and 10^5 , from bottom to top. The upper and lower dashed lines are $2T/(\gamma\nu k^2)$ and $T/(\gamma\nu k^2)$, respectively. The crossover between these asymptotes at $\Delta t \sim t_w$ ($k_n \sim k_w$) is clear. (b) Asymptotic time-delay limit, $\Delta t \gg t_L$, for $t_w = 1, 10, 10^2, 10^3, 10^4$, and 10^5 , from bottom to top. Dashed lines as in (a).

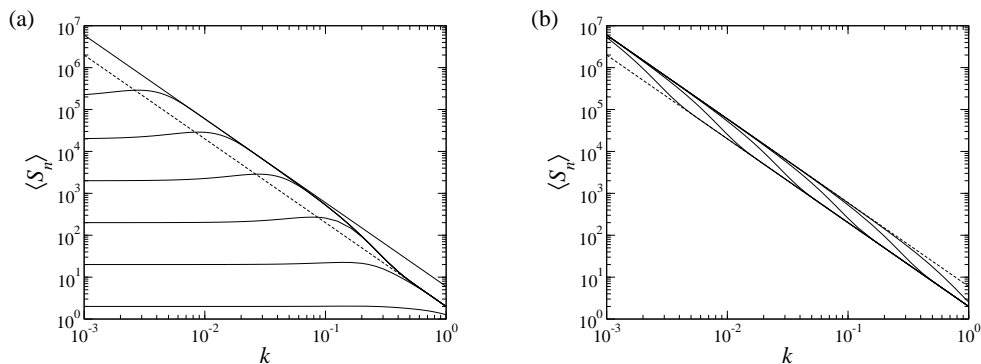


Figure 3. $T = 1$ evolution of the structure factor from an equilibrium initial condition at $T_0 = 5 > T$. (a) $t_w = 10$ and different time-delay values $\Delta t = 1, 10, 10^2, 10^3, 10^4$, and 10^5 , from bottom to top. The dashed lines are $2T/(\gamma\nu k^2)$ and $(T_0 + T)/(\gamma\nu k^2)$. (b) Asymptotic time-delay limit, $\Delta t \gg t_L$, for finite waiting-times $t_w = 1, 10, 10^2, 10^3, 10^4$, and 10^5 , from right to left. Dashed lines as in (a).

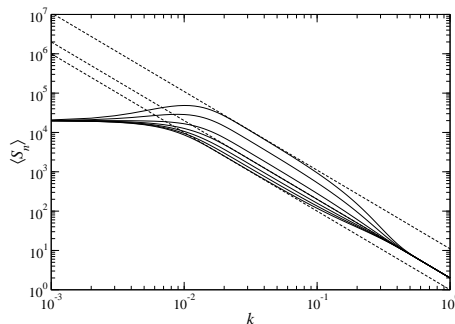


Figure 4. $T = 1$ evolution of the structure factor for different initial conditions, $T_0 = 0, 0.2, 0.5, 1, 2, 5, 10$, from bottom to top. $t_w = 10$ and $\Delta t = 10^4$. The dashed lines are $T/(\gamma\nu k^2)$ (middle) and $(T + T_0)/(\gamma\nu k^2)$ with $T_0 = 0$ (bottom) and $T_0 = 10$ (top).

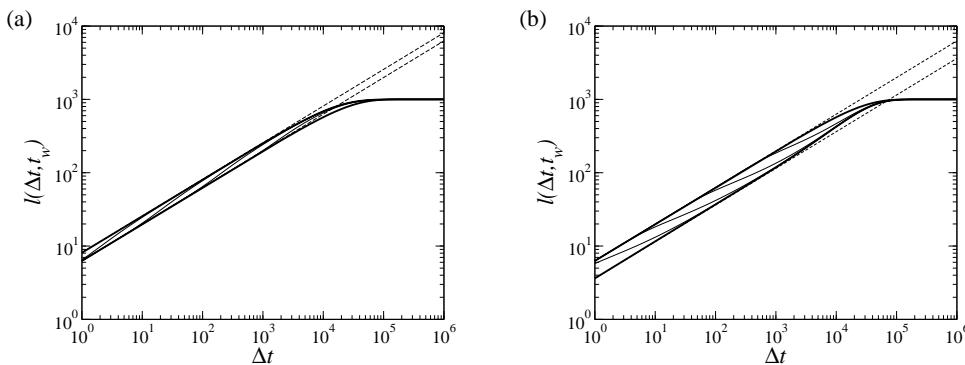


Figure 5. Aging of the two-times correlation length $l(\Delta t, t_w)$ for $L = 1000$. (a) $T_0 = 1 < T = 5$ and (b) $T_0 = 5 > T = 1$. The continuous curves are the full solution with $t_w = 1, 10, 10^2, 10^3$ from left to right in (a) and from bottom to top in (b). The thick curves correspond to $\lim_{t_w \gg t_L} l$ and $\lim_{t_w \ll t_L} l$; the former is located below for $T > T_0$ and above for $T < T_0$. The dashed straight lines correspond to the infinite size limit $L \rightarrow \infty$ taken at the outset and describe the $\Delta t^{1/2}$ growth law.

3. Two-times correlation length

A practical definition of a growing two-times correlation length, $l(\Delta t, t_w)$, is given by the fact that it marks the transition between the saturation regime at small k_n and the $1/k_n^2$ behavior at large k_n :

$$\langle S_{n=1} \rangle(\Delta t, t_w) = \lim_{\nu k_n^2 \Delta t \gg 1} \langle S_{n=L/l} \rangle(\Delta t, t_w). \quad (17)$$

This is similar to the numerical study in [13] for *disordered* elastic lines that, however, focuses only on a flat initial condition and does not take into account the waiting-time dependence. In that case, for $t_w = 0$ and $T_0 = 0$, a crossover from a power law growth to a logarithmic growth was found, which is related to the disordered energy landscape. In our case, without disorder, we found a waiting time crossover between two regimes marking the separation between *non-equilibrated* and *equilibrated* modes, as detailed in the following subsections.

3.1. Stationary limit.

In the stationary limit $t_w \gg t_L$ one finds

$$\lim_{t_w \gg t_L} l(\Delta t, t_w) = L \sqrt{1 - e^{-\Delta t/2t_L}}. \quad (18)$$

This expression varies from $\lim_{\Delta t \ll t_L} \lim_{t_w \gg t_L} l(\Delta t, t_w) = \sqrt{4\pi^2 \nu \Delta t}$ in the growing regime to $\lim_{\Delta t \gg t_L} \lim_{t_w \gg t_L} l(\Delta t, t_w) = L$ in the saturation regime. These limits correspond to the increases of the saturation value of the structure factor and the limit in which all the modes are equilibrated at the working temperature, respectively. The saturation time in the stationary regime corresponds to the time-delay when these limits are equal, $\Delta t_{t_w \gg t_L}^* = 2t_L$, and it is independent of T and T_0 .

3.2. Decay of the initial condition.

Setting $t_w = 0$ (or, more generally, $t_w \ll t_L$) one finds

$$\lim_{t_w \ll t_L} l(\Delta t, t_w) = L \sqrt{\frac{T_0 (1 - e^{-\Delta t/2t_L})^2 + T (1 - e^{-\Delta t/t_L})}{T_0 + T}}, \quad (19)$$

which varies between $\lim_{\Delta t \ll t_L} \lim_{t_w \ll t_L} l(\Delta t, t_w) = \sqrt{8\pi^2 \nu \Delta t T / (T_0 + T)}$ in the growing regime and $\lim_{\Delta t \gg t_L} \lim_{t_w \ll t_L} l(\Delta t, t_w) = L$ in the saturation regime. Equating these limits one finds the saturation time associated to the growing correlation length $\Delta t_{t_w=0}^* = (T_0/T + 1) t_L$, which depends on the initial condition.

3.3. Aging scaling.

In between the initial and the late stationary growths the two-times correlation length ages; *i.e.* it depends also on t_w . Equation (17) can be recast in a way that makes the scaling solution apparent

$$\frac{l^2}{t_w} \left[\left(\frac{T_0}{T} - 1 \right) e^{-4\pi^2 \nu t_w / l^2} + 2 \right] = g \left(\frac{T_0}{T}, \frac{\Delta t}{t_L}, \frac{t_w}{t_L} \right). \quad (20)$$

Indeed, this equation has a unique solution for l^2/t_w for each set of parameters in the right-hand-side. In the growing regime, $\Delta t \ll t_L$, for $T_0 > T$ the two-times length l moves from the upper asymptote, that corresponds to the $t_w = 0$ form in equation (19), to the lower one, that corresponds to the $t_w \gg t_L$ form in equation (18), at a Δt that increases with t_w . For $T_0 < T$ the trend reverses: l moves from the lower asymptote to the upper one, representing the $t_w \ll t_L$ and $t_w \gg t_L$ limits, respectively. The crossover between the two asymptotes occurs at a t_w -dependent Δt . More precisely, in the growing regime one has

$$l^2(\Delta t, t_w, T, T_0) = \begin{cases} c_\infty \Delta t & \Delta t \ll t_w \\ 2c_\infty T / (T_0 + T) \Delta t & \Delta t \gg t_w \end{cases} \quad (21)$$

with $c_\infty = 4\pi^2 \nu$. It is clear that the relative value of the prefactors depends on $T_0 > T$ or $T_0 < T$. The prefactor $c_0 \equiv 2c_\infty / (T_0/T + 1)$ vanishes at $T/T_0 \ll 1$, equals c_∞ at $T_0 = T$ and approaches $2c_\infty$ at $T/T_0 \gg 1$. The behaviour of the two-times dependent correlation length is summarized in Fig. 5 which displays the waiting-time dependent growth and subsequent saturation regime for two initial conditions (a) $T_0 < T$ and (b) $T_0 > T$.

One should notice that l increases monotonically with Δt and t_w before reaching saturation for both $T_0 > T$ and $T_0 < T$. This increase displays a multiplicative aging scaling behaviour between two asymptotes with opposite trend depending on $T_0 > T$ or $T_0 < T$. These kind of results were obtained, with additive aging scaling, in the out-of-equilibrium relaxation of mixtures of soft spheres and Lennard-Jones particles [18] and the 3d EA spin-glass [21, 19] after a quench from a high temperature (although the finite size saturation was not reached in these numerical studies). The heating case was not considered in these models.

4. Two-times roughness

The statics and equilibrium dynamics of elastic manifolds is usually understood in terms of the time, temperature and system size dependence of their averaged roughness or width [1]. In most studies of interface dynamics one compares the time-dependent configuration to the initial state, typically taken to be perfectly flat (equilibrium at zero temperature). The thermal averaged (one-time dependent) roughness is then

$$\langle w^2 \rangle(t) = L^{-d} \int d^d z \langle [x(\vec{z}, t) - x(\vec{z}, 0)]^2 \rangle, \quad (22)$$

where x is the height of the surface and \vec{z} is the position in the d -dimensional substrate typically with cubic geometry and linear size L .

The initial grow of the roughness is linear with time,

$$\lim_{\Delta t \rightarrow 0} \langle w^2 \rangle(t) = 2Tt, \quad (23)$$

which corresponds to a normal diffusion regime in which the beads on the line are still uncorrelated. Note that there is no ballistic regime since the EW equation represents overdamped Langevin dynamics. However, these inertial effects could be relevant in polymer – molecular – dynamics studies. The normal diffusion regime can be considered as a transient before the correlated dynamics of the interface is reached. In the *single particle* regime the roughness does not age. In the following we concentrate on the correlated aging dynamics of the line.

The thermal (and disorder averaged if random interactions are present) roughness follows the Family-Vicsek scaling [29], which means that it crosses over from growth to saturation at $t_x \sim L^z$ [1]:

$$\langle w^2 \rangle(t) \sim L^\zeta f(t/t_x), \quad (24)$$

where the scaling function obeys $f(y) \sim y^\beta$ for $y \ll 1$ and $f(y) \sim 1$ for $y \gg 1$, with ζ , β and $z = \zeta/\beta$ the roughness, growth and dynamic exponents, respectively. For the Edwards-Wilkinson (EW) line in $1 + d$ dimensions $\zeta = 2 - d$, $\beta = 1 - d/2$ and $z = 2$. In the presence of disorder, ζ is expected to take a ‘thermal’ value, ζ_{th} for $L < L_c(T)$ and a larger ‘disorder’ dominated value, ζ_{dis} for $L > L_c(T)$, both exponents being T -independent [1]. The other exponents, β and z may depend on T [11] or even logarithmic time-dependencies may exist [13].

We wish to take into account the waiting-time t_w and consider also more general initial conditions. To this end we generalize the definition in equation (22) to

$$\langle w^2 \rangle(t, t_w) \equiv \frac{1}{L} \int_0^L dz \langle [\delta x(z, t) - \delta x(z, t_w)]^2 \rangle = \frac{2}{L} \sum_{n=1}^{\infty} \langle S_n \rangle(t, t_w) \quad (25)$$

with $\delta x(z, t)$ defined in equation (3) and specialized to $d = 1$. Note that the zero mode is not included in the sum.

In general, one expects the dynamics to become stationary after an equilibration time t_L ; the generalized thermal averaged roughness should then scale as in equation (24) with t replaced by Δt . For not too short L , t_L may become very long and the dynamics

might remain non-stationary with $\langle w^2 \rangle$ depending on t_w explicitly for $t_w < t_L$. In [9] we conjectured that the scaling of the roughness in the *non-equilibrium relaxation* of *infinitely* long elastic lines with or without quenched disordered potentials follows the law

$$\langle w^2 \rangle(\Delta t, t_w) \sim \ell^\zeta(t_w) \mathcal{F} \left[\frac{\ell(t)}{\ell(t_w)} \right] \quad (26)$$

with $\ell(t)$ a growing length (dimensions are restored by prefactors that we omit) and \mathcal{F} a scaling function. For each waiting-time this form approaches a stationary growth regime $\langle w^2 \rangle \sim \ell^\zeta(\Delta t)$ when $t_w \ll \Delta t \ll t_L$ if $\mathcal{F}(y) \sim y^\zeta$ for $y \gg 1$. It is also reasonable to assume $\mathcal{F}[\ell(t)/\ell(t_w)] \sim \ell^\zeta(\Delta t)$ for $\Delta t \ll t_w$, that leads to a stationary growth of the averaged roughness at very short time-delays. This result is explicitly realized in the power law case. One may extend this conjecture to apply to manifolds with internal dimension D in a transverse space with dimension d . The functional form of the growing length, ℓ , the scaling function, \mathcal{F} , and the values of the exponent are expected to vary from case to case.

In a series of numerical studies one established that, in the numerically accessible times, the quenched dynamics of a *disordered* 1 + 1 lattice model [8, 9] satisfies the scaling in equation (26) with $\ell(t) \sim t^{\alpha/\zeta}$ and α/ζ a rather *small* exponent. A crossover to a logarithmic time-dependence [13] is not excluded although it was not seen in the out-of-equilibrium relaxation. It was shown that the roughness ages, by crossing over between two asymptotes, for $\Delta t \gg t_w$ and $\Delta t \ll t_w$, thus having

$$\langle w^2 \rangle \sim c_{1,2}(T) \Delta t^{\alpha(T)}, \quad \text{with } \alpha(T) < \beta_{EW} = 0.5, \quad (27)$$

and different proportionality constants. The waiting-time dependence appears in the way these asymptotes are approached. $\alpha(T)$ is a generalization of the growth exponent, β , in surface growth literature, and $\alpha(T) < \beta_{EW}$, with β_{EW} the Edwards-Wilkinson value, reflects that quenched disorder slows down the dynamics.

In order to better understand this aging behaviour, trying to separate the effects due to disorder from those related to the intrinsic elastic character of the line, we present here results for the EW case in 1 + 1 dimensions *without disorder*. In this case the two-times averaged roughness is given by

$$\langle w^2 \rangle(\Delta t, t_w) = \frac{6w_0^2}{\pi^2} \sum_{n=1}^{\infty} b_n(\Delta t, t_w) + \frac{6w_\infty^2}{\pi^2} \sum_{n=1}^{\infty} a_n(\Delta t, t_w), \quad (28)$$

$$n^2 a_n(\Delta t, t_w) = 2 \left(1 - e^{-n^2 \frac{\Delta t}{2t_L}} \right) \left(1 - e^{-n^2 \frac{t_w}{t_L}} \right) + \left(1 - e^{-n^2 \frac{\Delta t}{t_L}} \right) e^{-n^2 \frac{t_w}{t_L}}, \quad (29)$$

$$n^2 b_n(\Delta t, t_w) = \left(1 - e^{-n^2 \frac{\Delta t}{2t_L}} \right)^2 e^{-n^2 \frac{t_w}{t_L}}, \quad (30)$$

where we used the definitions

$$w_0^2 \equiv T_0 L / (12\gamma\nu), \quad w_\infty^2 \equiv T L / (12\gamma\nu). \quad (31)$$

The averaged two-times roughness can be written in terms of the scaled times

$$\langle w^2 \rangle(\Delta t, t_w) = \langle w^2 \rangle \left(\frac{\Delta t}{t_L}, \frac{t_w}{t_L} \right) = \langle w^2 \rangle \left(\frac{\Delta t}{t_L}, \frac{\Delta t}{t_w} \right) \quad (32)$$

while temperatures appear separately, through w_0^2 and w_∞^2 . We first focus on the time-dependence of the roughness of infinite lines, $L \rightarrow \infty$, before testing the dynamics at different asymptotic limits, and we later reverse the order of limits by considering finite lines, $L < \infty$. We display the analytic results in Figs. 6-8 in which we approximate the series in the analytic expressions by using finite sums, $\sum_{n=0}^{\infty} \rightarrow \sum_{n=0}^M$, with $M = 1000$ in all cases, except for lines with $L = 3000$ for which we used $M = 500$.

4.1. Infinite system size.

By taking $L \rightarrow \infty$ at the outset t_L diverges and

$$\lim_{L \rightarrow \infty} \langle w^2 \rangle(\Delta t, t_w) = \sqrt{\frac{2t_w}{\pi\gamma^2\nu}} \left[(T - T_0) \left(1 + \sqrt{\frac{\Delta t}{t_w} + 1} - \sqrt{\frac{2\Delta t}{t_w} + 4} \right) + 2T \sqrt{\frac{\Delta t}{2t_w}} \right], \quad (33)$$

which can be written in the scaling form

$$\lim_{L \rightarrow \infty} \langle w^2 \rangle(\Delta t, t_w) = t_w^{1/2} \tilde{w}^2 \left(\frac{\Delta t}{t_w} \right), \quad (34)$$

and admits the scaling form in equation (26) with $\ell(t) \sim t^{1/2}$. Comparing now Δt to a long waiting-time, that is to say taking $\Delta t \ll t_w$, one finds that the waiting-time dependence determines the crossover between two square-root dependencies in Δt with different, temperature-dependent, prefactors:

$$\langle w^2 \rangle(\Delta t, t_w) = \begin{cases} c_\infty^{w^2}(T) \Delta t^{1/2} & \Delta t \ll t_w \\ c_0^{w^2}(T, T_0) \Delta t^{1/2} & \Delta t \gg t_w \end{cases} \quad (35)$$

with $c_0^{w^2} = [T + T_0(\sqrt{2} - 1)]\sqrt{2/(\pi\gamma^2\nu)}$ and $c_\infty^{w^2} = 2T/\sqrt{\pi\gamma^2\nu}$. Note that $c_0^{w^2} < c_\infty^{w^2}$ for $T > T_0$, the two constants are identical at $T = T_0$, and $c_0^{w^2} > c_\infty^{w^2}$ for $T < T_0$. The two trends are shown in Fig. 7 (b). These results are of the generic form proposed in [9], see equation (26), with $\alpha = \beta_{EW} = 1/2$ independently of temperature, $\ell(t) \sim t^{1/2}$, and temperature dependencies of the constants made explicit.

4.2. Finite lines

For finite L , by considering the long waiting-time limit $t_w \gg t_L$ the stationary Family-Vicsek scaling form (24) is recovered. Indeed, one has that

$$\lim_{t_w \gg t_L} \langle w^2 \rangle(\Delta t, t_w) = w_\infty^2 \sum_{n=1}^{\infty} \frac{12}{\pi^2 n^2} \left(1 - e^{-n^2 \Delta t / 2t_L} \right). \quad (36)$$

This form for the stationary roughness contains the growing regime where $\lim_{\Delta t \ll t_L} \lim_{t_w \gg t_L} \langle w^2 \rangle = c_\infty^{w^2}(T) \Delta t^{1/2}$ as in eq. (35), and later crosses over to the saturation value

$$\lim_{\Delta t \gg t_L} \lim_{t_w \gg t_L} \langle w^2 \rangle(\Delta t, t_w) = 2w_\infty^2 = \frac{TL}{6\gamma\nu}. \quad (37)$$

On the other hand, the averaged roughness at $t_w = 0$ for finite L , or more precisely for $t_w \ll t_L$, also follows the familiar Family-Vicsek scaling form (24). In this case, the

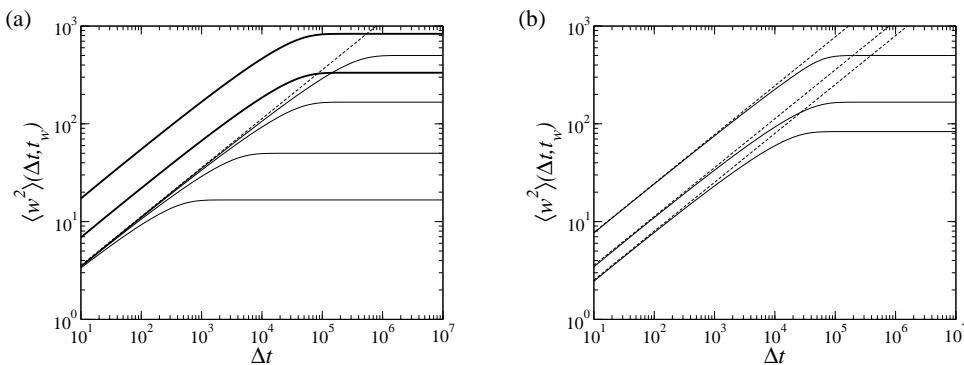


Figure 6. (a) Stationary roughness ($t_w \gg t_L$) as a function of Δt . Thin lines correspond to different system sizes $L = 100, 300, 1000, 3000$, from bottom to top all at $T = 1$. Thick lines correspond to $L = 1000$ and $T = 2$ (bottom) and $T = 5$ (top). Note that the saturation time t_x does not depend on T . The dashed line is the limit $L \rightarrow \infty$ for $T = 1$. (b) Roughness with $t_w = 0$, $T = 1$, and different initial conditions corresponding, from bottom to top, to $T_0 = 0, 1$, and 5 . In the $t_w \gg t_L$ limit, the roughness goes to its stationary solution, also given by the curve in the middle. Dashed lines correspond to $\lim_{L \rightarrow \infty} \langle w^2 \rangle$ given by equation (35).

roughness crosses over from a growing regime $\lim_{\Delta t \ll t_L} \lim_{t_w \ll t_L} = c_0^{w^2}(T, T_0) \Delta t^{1/2}$ to a saturation value which depends on the initial condition,

$$\lim_{\Delta t \gg t_L} \lim_{t_w \ll t_L} \langle w^2 \rangle(\Delta t, t_w) = w_0^2 + w_\infty^2 = \frac{(T_0 + T)L}{12\gamma\nu}. \quad (38)$$

Note that the saturation value reached in the stationary regime, after having taken $t_w \gg t_L$, is *twice* the saturation value obtained from the flat initial condition $T_0 = 0$. This result demonstrates how important it is to be careful with the choice of t_w to ensure that one has reached the stationary regime when using numerical simulations.

When considering all the waiting-time dependence the roughness interpolates between the different limiting values given above. For sufficiently large but finite systems it is possible to find a well defined aging of the growing regime when both Δt and t_w are smaller than the saturation time. In this case one recovers the scaling behaviour found in the infinite size system, equations (33) and (35). For finite L though this scaling form terminates at a characteristic time-delay, $t_x(t_w) \propto t_L$ – see below – and $\langle w^2 \rangle$ later saturates at a waiting-time-dependent value, which interpolates between the two limiting saturation values, equations (37) and (38). These results are the same as the ones obtained using the reverse order of time limits, see (37) and (38). The t_w -dependence in the saturation regime is shown in Fig. 8.

Although in the previous analysis we used t_L as a reference time to determine the long time-delay limit. One can be more precise and define a waiting-time dependent saturation time, $t_x(t_w)$. Equating the growing and saturation behaviour of the roughness, one can extract the saturation times at two extreme values of t_w :

$$t_x(t_w \ll t_L) = \frac{\pi}{288\nu} \left[\frac{T + T_0}{T + T_0(\sqrt{2} - 1)} \right]^2 L^2, \quad (39)$$

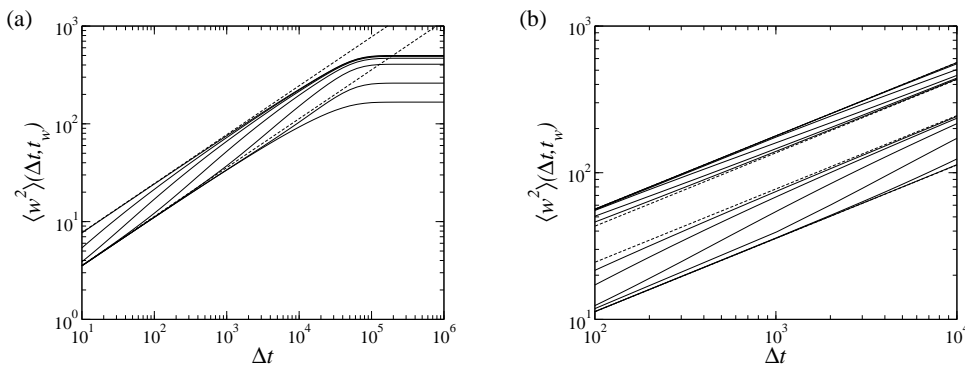


Figure 7. Aging of the two-times roughness, $t_w = 0, 10^0, 10^1, 10^2, 10^3, 10^4, 10^5$. (a) $L = 1000, T_0 = 5$ and $T = 1$, t_w increases from top to bottom. The upper and lower dashed lines correspond to $L \rightarrow \infty$ with $t_w = 0$ and $t_w \gg t_L$, respectively. (b) $L \rightarrow \infty$; t_w increases from top to bottom in the lower set of curves ($T_0 = 5$ and $T = 1$) and from bottom to top in the upper set of curves ($T_0 = 1$ and $T = 5$).

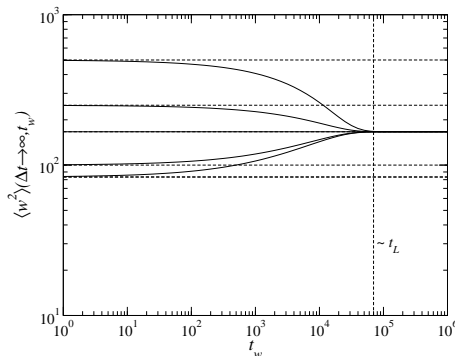


Figure 8. Aging of the roughness at saturation, $\lim_{\Delta t \gg t_L} w^2(\Delta t, t_w)$. $T = 1$ and $T_0 = 0, 0.2, 1, 2, 5$ from bottom to top. Dashed lines correspond to $(T + T_0)L / (12\gamma\nu)$.

$$t_x(t_w \gg t_L) = \frac{\pi}{144\nu} L^2. \quad (40)$$

Both results are proportional to t_L , and $t_x(t_w)$ interpolates between these two values. This justifies the use of t_L as the reference time-delay before saturation; the prefactors are finite for all T and T_0 , the former is larger (smaller) for $T < T_0$ ($T > T_0$) and become identical at $T = T_0$. The saturation time and its dependence on L are visible in Figs. 6 and 7 (a).

4.3. Scaling relations

Here we present the main results concerning the aging properties of the roughness. We have shown for the aging regime that

$$\begin{aligned} t_x &\sim a(T) L^z, & z &= 2, \\ \langle w^2 \rangle_{\Delta t \gg t_x} &\sim L^\zeta, & \zeta &= 1, \\ \langle w^2 \rangle_{\Delta t \ll t_x} &\sim c(T, T_0, \Delta t/t_w) t_w^\beta, & \beta &= 1/2, \end{aligned}$$

see equations (39) and (40), equation (31) and equation (35), respectively. The prefactor $c(T, T_0, \Delta t/t_w)$ approaches $c_\infty^{w^2}(T)(\Delta t/t_w)^{1/2}$ and $c_0^{w^2}(T, T_0)(\Delta t/t_w)^{1/2}$, for $\Delta t \ll t_w$ and $\Delta t \gg t_w$, respectively. These relations imply

$$t_x \sim a(T)(w_\infty^2)^{z/\zeta} \sim [a(T)\zeta/z w_\infty^2]^{z/\zeta}, \quad (41)$$

where we have used that $\langle w^2 \rangle_{\Delta t \gg t_x} \sim w_\infty^2$ for simplicity. From matching the end of the growth regime with saturation at $t_w \ll \Delta t = t_x$ one has

$$c(T, T_0, \Delta t/t_w) t_x^\beta \sim c_0^{w^2}(T, T_0) t_x^\beta \sim w_\infty^2 \quad \text{and} \quad \beta = \zeta/z, \quad (42)$$

(the latter condition is satisfied by the values of the exponents found). Thus one finally has that

$$a(T)^{-\zeta/z} = c_0^{w^2}(T, T_0). \quad (43)$$

Note that the exponents take simple values in the EW case but, in general, they can be T -dependent (not ζ) [11].

5. Mean-squared and center-of-mass displacements

The two-times roughness, equation (25), may also be written as

$$\begin{aligned} \langle w^2 \rangle(t, t_w) &= \langle B \rangle(t, t_w) - \langle D \rangle(t, t_w) \\ &= \left\langle [x(z, t) - x(z, t_w)]^2 \right\rangle - \left\langle [\overline{x(t)} - \overline{x(t_w)}]^2 \right\rangle, \end{aligned} \quad (44)$$

where $\langle B \rangle$ and $\langle D \rangle$ represent the averaged mean-squared-displacement of the differential line segments and the center of mass of the line, respectively, see Fig. 1. This relation simply states that the roughness is a measure of the fluctuations around the center of mass of the line.

It is simple to show that the center of mass diffuses normally. Indeed, integrating equation (1) over the line length one has $\partial_t \bar{x}(t) = \xi'(t)$, with $\xi'(t) = \frac{1}{L} \int_0^L dz \xi(z, t)$, $\langle \xi'(t) \rangle = 0$, $\langle \xi'(t) \xi'(t') \rangle = \frac{2T}{\gamma L} \delta(t - t')$, and

$$\langle D \rangle(t, t_w) = \langle D \rangle(\Delta t) = \frac{2T}{\gamma L} \Delta t. \quad (45)$$

The diffusion constant is an inverse function of the line length.

In previous studies of the elastic line out-of-equilibrium dynamics [8, 16] one focused on the mean-squared-displacement that, in the case of the EW line, is just given by $\langle B \rangle(t, t_w) = \langle w^2 \rangle(t, t_w) + 2T/(\gamma L) \Delta t$. At short time-delay w^2 and B are practically identical while in the saturation regime the displacement is just given by the normal diffusion law.

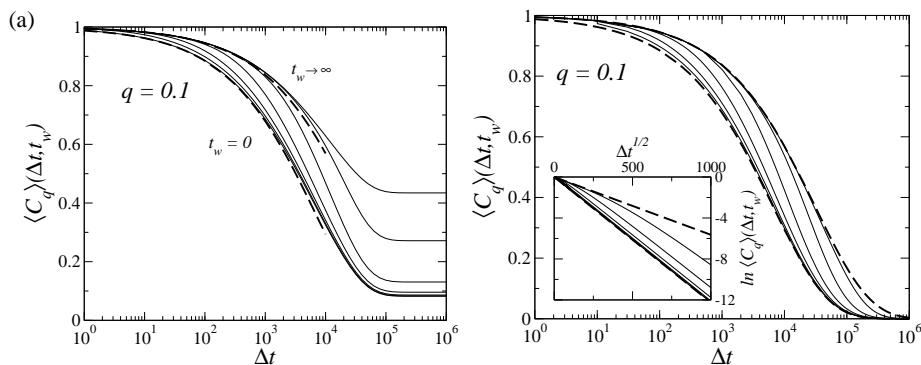


Figure 9. The wave-vector dependent correlation function defined in equation (47) and given in terms of $\langle w^2 \rangle$ by equation (48) for a Gaussian process. $\langle C_q \rangle$ at $T_0 = 5$, $T = 1$, $q = 0.1$ and $t_w = 0, 1, 10, 10^2, 10^3, 10^4$, and 10^5 . (a) $L = 1000$. The thick dashed lines correspond to the limits $L \rightarrow \infty$ with $t_w = 0$ (lower curve) and $t_w \gg t_L$ (upper curve). (b) $L \rightarrow \infty$ limit; the rest of the parameters are as in panel (a). The inset shows the same curves in a different scale, *i.e.* $\ln \langle C_q \rangle$ vs. $\Delta t^{1/2}$.

6. The incoherent scattering function

The dynamics of glassy systems is usually analyzed in terms of the wave-vector dependent incoherent scattering function:

$$\langle C_q \rangle(t, t_w) = N^{-1} \sum_{i=1}^N \langle e^{i\vec{q}[\vec{r}_i(t) - \vec{r}_i(t_w)]} \rangle \quad (46)$$

with N the total number of particles, $\vec{r}_i(t)$ the time-dependent position of particle i and \vec{q} a wave-vector. C_q is measured numerically and experimentally. In the context of elastic lines, one defines

$$\langle C_q \rangle(\Delta t, t_w) = L^{-1} \int dz \langle e^{iq[\delta x(z, t) - \delta x(z, t_w)]} \rangle. \quad (47)$$

In the EW case the displacement in the exponential is a Gaussian random variable and

$$\langle C_q \rangle(\Delta t, t_w) = e^{-\frac{q^2}{2} \langle w^2 \rangle(\Delta t, t_w)}. \quad (48)$$

The incoherent scattering function $\langle C_q \rangle$ is simply related to the roughness, $\langle w^2 \rangle$, analyzed in Sect. 4. Figure 9 displays the time-delay decay of $\langle C_q \rangle$ at $q = 0.1$ using several waiting-times. For finite lines the saturation in $\langle w^2 \rangle$ is attained at sufficiently long Δt and the correlation reaches a waiting-time dependent plateau with its height increasing with t_w , Fig.9 (a). For sufficiently long lines the saturation regime can be pushed beyond the observed time-delay window as exemplified in the limit $L \rightarrow \infty$, Fig. 9 (b). In Fig. 10 we display the dependence of $\langle C_q \rangle$ on Δt for fixed t_w and different values of q . One notices that the small q correlations saturate in the Δt window while large q correlations relax to zero. This is to be expected since $q^2 w_\infty^2$ scales as $q^2 L$ and the effect of decreasing q is like decreasing L . Note the similarity between these plots and light-scattering measurements in clay suspensions (laponite) [17].

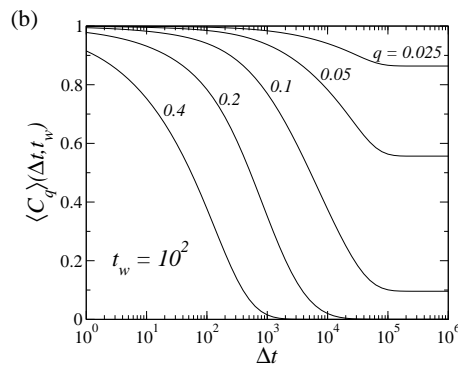


Figure 10. $\langle C_q \rangle$ for $L = 1000$, $t_w = 10^2$ and different wave-vectors q as indicated. $T_0 = 5$ and $T = 1$.

7. Response functions and FDT

We now compute the linear response function of several observables related to the two-times correlations studied above.

7.1. Center of mass response

In order to evaluate the linear response we have to switch on a perturbing field coupled to the observable of interest. Let us start with the linear response function associated with the center of mass diffusion, $\langle \chi^D \rangle$. The effect of a perturbing field, h , applied on the center of mass after time t_w is described by the term

$$\mathcal{H}^D = -h L \bar{x}(t) \theta(t - t_w) = -h \int_0^L dz x(z, t) \theta(\Delta t) \quad (49)$$

that is added to the energy. Calling $\bar{x}^h(t)$ and $\bar{x}(t)$ the center of mass position with and without field, respectively, the linear response function is

$$\langle \chi^D \rangle(t, t_w) = \frac{1}{hL} \langle \bar{x}^h(t) - \bar{x}(t) \rangle \quad (50)$$

which depends only on the time difference and satisfies the FDT for any t and t_w ,

$$\langle D \rangle(\Delta t) = 2T \langle \chi^D \rangle(\Delta t). \quad (51)$$

7.2. Roughness response

The energy contribution of a field conjugated to the roughness is

$$\mathcal{H}^{w^2} = -h \int_0^L dz [x(z, t) - \bar{x}(t)] s(z) \theta(\Delta t). \quad (52)$$

As usual, $s(z)$ are *i.i.d.* quenched random variables taking values $s(z) = \pm 1$ with equal probability: $\langle s(z) \rangle = 0$ and $\langle s(z) s(z') \rangle = \delta(z - z')$. The associated response function is

$$\langle \chi^{w^2} \rangle(t, t_w) = \frac{1}{hL} \left\langle \int_0^L dz [\delta x^h(z, t) - \delta x(z, t)] s(z) \right\rangle$$

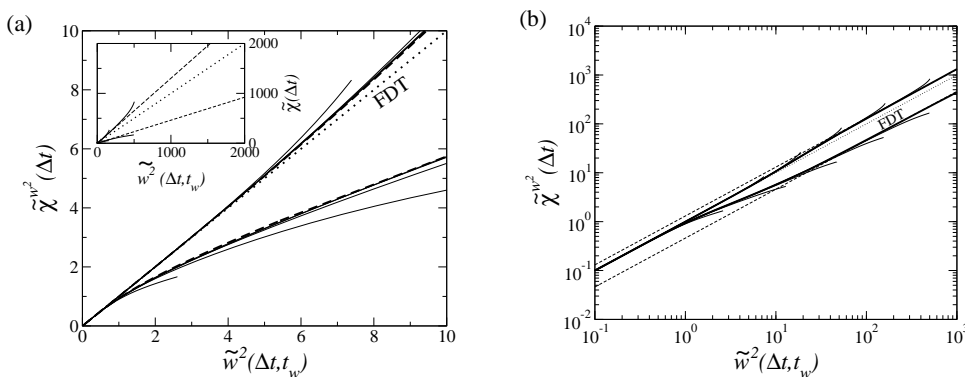


Figure 11. Violation of the FDT in the aging regime of the EW equation. The parametric plots $\tilde{\chi}^{w^2} = 1/(2T_{eff}) \tilde{w}^2$ are constructed from the scaled variables defined by $\tilde{w}^2 = t_w^{-1/2} \langle w^2 \rangle$ and $\tilde{\chi}^{w^2} = t_w^{-1/2} \langle \chi^{w^2} \rangle$. (a) The parametric plot in linear scale showing the departure from the FDT (dotted line). Upper and lower sets of curves correspond to $T_0 = 1, T = 5$ and $T_0 = 5, T = 1$, respectively. Thick dashed lines represent the $L \rightarrow \infty$ limit. Thin lines are for $L = 1000$ and different waiting-times, and show the finite size signature in the FDT parametric plot. The inset shows the large scale violation of FDT with two straight lines, which corresponds to effective temperatures larger (for $T_0 > T$) and smaller (for $T_0 < T$) than the working temperature T . The initial FDT regime is not clearly observed in this scale. (b) The parametric plot in log-log scale showing that the violation of the FDT is given by equation (63) at $\Delta t \gg t_w$.

$$= \frac{2}{h} \sum_{n=1}^{\infty} \langle [c_n^h(t) - c_n(t)] s_n \rangle, \quad (53)$$

with s_n defined through $\delta s(z) = s(z) - \bar{s} = \sum_{n=-\infty}^{\infty} s_n e^{ik_n z}$. Here $\langle \dots \rangle$ also indicates the average over the s_n distribution. One finds

$$\langle \chi^{w^2} \rangle(\Delta t) = \left(1 - e^{-\nu k_n^2 \Delta t} \right) \quad (54)$$

where we used $\langle s_n^2 \rangle = 1/L$. Interestingly enough, the linear response is stationary for all t_w while the roughness is not. Therefore, the FDT is not respected for waiting-times $t_w \ll t_L$, and its modification is discussed in Sect. 7.4 and Fig. 11. In the stationary limit $t_w \gg t_L$ the roughness becomes stationary and the FDT holds, *i.e.*

$$\lim_{t_w \gg t_L} \langle w^2 \rangle(\Delta t, t_w) = 2T \langle \chi^{w^2} \rangle(\Delta t). \quad (55)$$

This statement also implies that the FDT does not hold for $t_w = 0$ and $T = 0$, pointing again that one should be careful with the choice of t_w and the stationary limit.

7.3. Mean-squared-displacement response

The effect of a perturbing field conjugated to the mean-squared-displacement is represented by

$$\mathcal{H}^B = -h \int_0^L dz x(z, t) s(z) \theta(\Delta t), \quad (56)$$

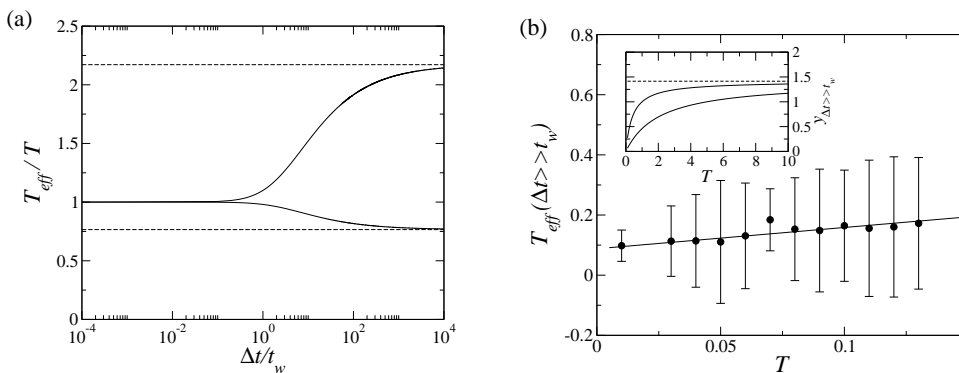


Figure 12. The effective temperature T_{eff} characterizing the violation of the FDT in the EW equation. (a) Evolution with the rescaled time $\Delta t/t_w$ showing that FDT holds when $\Delta t \ll t_w$ and it does not hold when $\Delta t \gg t_w$. Upper and lower curves correspond to $T_0 = 5, T = 1$ and $T_0 = 1, T = 5$, respectively. The dashed lines represent the limit $\Delta t \gg t_w$ in equation (63). (b) $T_{eff}(\Delta t \gg t_w)$ vs. T for $T_0 = 0.3$ (continuous line) compared to the data in Fig. 25 in [10] describing the effective temperature of independent elastic lines (with the Josephson correction to the elasticity) moving in a *quenched random environment*. The inset shows $y_{\Delta t \gg t_w} = \lim_{\Delta t \gg t_w} T/T_{eff}(T)$ as a function of temperature for $T_0 = 1, T = 5$ (lower curve) and $T_0 = 5, T = 1$ (upper curve). The dashed line is the limit $T \gg T_0$.

with the random $s(z)$ distributed as above. The linear response function is defined as

$$\begin{aligned} \langle \chi^B \rangle(t, t_w) &= \frac{1}{hL} \left\langle \int_0^L dz [x^h(z, t) - x(z, t)] s(z) \right\rangle \\ &= \langle \chi^{w^2} \rangle(t, t_w) + \frac{\langle \bar{s} \rangle}{h} [\bar{x}^h(t) - \bar{x}(t)]. \end{aligned} \quad (57)$$

The last term of this expression represents the center-of-mass response to a field of intensity $h' = h/\langle \bar{s} \rangle$. Thus, in the long waiting-time limit, $\langle \chi^B \rangle$ is also stationary and simply related to the roughness and center-of-mass responses,

$$\langle \chi^B \rangle(\Delta t) = \langle \chi^{w^2} \rangle(\Delta t) + \langle \chi^D \rangle(\Delta t). \quad (58)$$

In this case, the FDT is not satisfied in general but in the stationary regime it is:

$$\lim_{t_w \gg t_L} \langle B \rangle(t, t_w) = \langle B \rangle(\Delta t) = 2T \langle \chi^B \rangle(\Delta t). \quad (59)$$

7.4. FDT and effective temperature

Since FDT holds for $t_w \gg t_L$, it is interesting to study the violation of the FDT at finite t_w . To this end we use the $L \rightarrow \infty$ limit, where the roughness takes the scaling form in equation (33), and

$$\lim_{L \rightarrow \infty} \langle \chi^{w^2} \rangle(\Delta t) = t_w^{1/2} \tilde{\chi}^{w^2} \left(\frac{\Delta t}{t_w} \right) \quad \text{with} \quad \tilde{\chi}^{w^2} \left(\frac{\Delta t}{t_w} \right) = \sqrt{\frac{1}{\pi \gamma^2 \nu} \frac{\Delta t}{t_w}}. \quad (60)$$

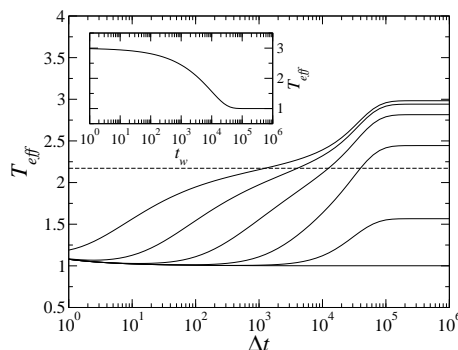


Figure 13. The effective temperature T_{eff} as a function of time-delay for $t_w = 1, 10, 10^2, 10^3, 10^4$ and 10^5 from top to bottom; $L = 1000$, $T_0 = 5$ and $T = 1$. The dashed line is $\lim_{t_w \ll \Delta t} \lim_{L \rightarrow \infty} T_{eff}$ [the same dashed curve as in Fig. 12 (a)] and justifies the shoulder for small t_w . The inset shows $T_{eff}(\Delta t = 10^6 \gg t_L, t_w)$ as a function of t_w ; it is clear that at sufficiently long t_w one recovers $T_{eff} = T$.

Once we eliminated the $t_w^{1/2}$ diffusive factor one can associate the ratio between \tilde{w}^2 and $\tilde{\chi}^{w^2}$ with an effective temperature [8, 10],

$$\tilde{\chi}^{w^2} = \frac{1}{2T_{eff}} \tilde{w}^2. \quad (61)$$

which, in this case, depends on T , T_0 , Δt and t_w . From equation (33) we obtain

$$T_{eff} = T \left[1 + \frac{T - T_0}{T} \left(\sqrt{\frac{t_w}{2\Delta t}} + \frac{1}{\sqrt{2}} \sqrt{1 + \frac{t_w}{\Delta t}} - \sqrt{1 + \frac{2t_w}{\Delta t}} \right) \right]. \quad (62)$$

In the case $T = T_0$ one recovers $T_{eff} = T$ as expected. One can check that $T_{eff} > T$ or $T_{eff} < T$ whenever $T_0 > T$ or $T_0 < T$. In the two extreme cases $\Delta t \ll t_w$ and $\Delta t \gg t_w$ one finds two waiting-time *independent* values of T_{eff} :

$$T_{eff} = \begin{cases} T & \Delta t \ll t_w, \\ T + (T_0 - T) \left(1 - \frac{1}{\sqrt{2}} \right) & \Delta t \gg t_w, \end{cases} \quad (63)$$

see Figs. 11 and 12, indicating that fast modes are equilibrated while the slow ones are not. These results are very similar to what has been found numerically for the dynamics of elastic lines in a quenched random potential [8] and in models of *interacting* elastic lines in quenched random environments that describe the vortex glass in high T_c superconductors [10], see Fig. 12. Note that the waiting-time dependence in T_{eff} only marks the crossover between the two asymptotic regimes. At still longer Δt such that $\Delta t \gg t_x \sim t_L$ the FDT result, $T_{eff} = T$, is recovered. This is shown in Fig. 13, a result that, once again, resembles what was found in laponite [30].

8. Fluctuations

Upto this point we studied the scaling properties of several two-times quantities averaged over the length of the line *and* thermal noise. A more refined investigation of interface dynamics, currently done theoretically and experimentally, deals with the fluctuating

quantities such as the distribution functions of the width of heights [20], the density of local maxima or minima of heights [31, 32], the statistics of first passage times, *etc.* It is also clear by now that to gain a complete understanding of glassiness one should also understand the dynamic fluctuations [21, 22]. In the glassy context one expects that the competition between different time or length scales in the system reflects in the way the probability distribution functions (pdfs) behave.

Rácz proposed that, for elastic systems, the scaling form of the distribution function characterizing the roughness fluctuations may serve to classify the systems into different universality classes [20]. For a given system size the pdf of the roughness, $P_L(w^2)$, scales as [33]

$$w_\infty^2 P_L(w^2) = \Phi\left(\frac{w^2}{w_\infty^2}\right), \quad (64)$$

in the saturation regime, and the form of the scaling function was shown to be useful to differentiate between the EW and KPZ universality classes [20]. The full stationary pdf of the EW roughness was also computed, showing the same scaling behavior as in equation (64). These works considered only the $t_w = 0$ case with a flat initial condition ($T = 0$). Recently, a simulation study of a disordered elastic-line model defined on the lattice demonstrated that the scaling form of the distribution function must be modified to include the aging effects [9].

In the body of this Section we analyze the thermal noise-induced dynamic fluctuations of the two-times quantities defined previously during the aging relaxation.

8.1. Roughness distribution

Rewriting the roughness w^2 in terms of $u(z, t, t_w) = x(z, t) - x(z, t_w)$, the pdf of the two-times roughness, $P_L(w^2)$, is given by

$$P_L(w^2) = \int \mathcal{D}[x] \mathcal{D}[x'] \delta\left[w^2 - \left(\overline{u^2(t, t_w)} - \overline{u(t, t_w)}^2\right)\right] p(x, t; x', t_w),$$

where $\mathcal{D}[x]$ is the measure over x configurations; x and x' represent the configurations at time t and t_w , respectively; and $p(x, t; x', t_w)$ is their joint probability density. The Laplace transform $G_L(\lambda) = \int_0^\infty d\alpha P_L(\alpha) e^{-\lambda\alpha}$, can be written as the path integral

$$G_L(\lambda) = \int \mathcal{D}[x] \mathcal{D}[x'] p(x, t; x', t_w) e^{-\lambda(\overline{u^2(t, t_w)} - \overline{u(t, t_w)}^2)}. \quad (65)$$

Using the independent Fourier modes defined in equation (3)

$$G_L(\lambda, t, t_w) = \mathcal{N} \int \prod_{n=1}^{\infty} dc_n dc_n^* dc'_n dc_n'^* p^2[c_n(t), c_n(t_w)|c_n(0)] e^{-2\lambda|c_n(t) - c_n(t_w)|^2}, \quad (66)$$

where \mathcal{N} is a normalization factor ensuring $G_L(0) = 1$ at all times. The quantity $p[c_n(t), c_n(t_w)|c_n(0)]$ is the joint probability density of having c_n at time t and $c'_n = c_n(t_w)$ at time t_w , given the initial condition $c_n(0)$. This quantity can be expressed as $p[c_n(t), c_n(t_w)|c_n(0)] = p[c_n(t)|c_n(t_w)]p[c_n(t_w)|c_n(0)]$, where $p[c_n(t)|c_n(t')]$ is the conditional probability of evolving from $c_n(t')$ to $c_n(t)$ in the time interval $t - t'$. This

states that the joint probability is simply the product of the probabilities of evolving from the initial condition to the intermediate configuration $c_n(t_w)$, and from there to the configuration $c_n(t)$, and satisfies

$$p[c_n(t)|c_n(0)] = \int dc'_n dc_n^* p[c_n(t), c_n(t_w)|c_n(0)]. \quad (67)$$

The conditional probability $p[c_n(t)|c_n(t')]$ is given by the complex Gaussian

$$p[c_n(t)|c_n(t')] = \frac{1}{2\pi\sigma_n^2(t-t')} e^{-\frac{|c_n(t)-c_n(t')e^{-\nu k_n^2(t-t')}|^2}{2\sigma_n^2(t-t')}}, \quad (68)$$

where

$$\sigma_n^2(t-t') = \frac{T}{L\gamma\nu k_n^2} \left[1 - e^{-2\nu k_n^2(t-t')}\right]. \quad (69)$$

Therefore, the joint probability function for the Fourier modes at times t and t_w becomes

$$p[c_n(t), c_n(t_w)|c_n(0)] = \frac{e^{-\frac{|c_n(t)-c_n(t_w)e^{-\nu k_n^2\Delta t}|^2}{2\sigma_n^2(\Delta t)}} e^{-\frac{|c_n(t_w)-c_n(0)e^{-\nu k_n^2 t_w}|^2}{2\sigma_n^2(t_w)}}}{(2\pi)^2\sigma_n^2(\Delta t)\sigma_n^2(t_w)}. \quad (70)$$

After some algebra one finds the normalization factor $\mathcal{N} = \prod_{n=1}^{\infty} 16\pi^2\sigma_n^2(\Delta t)\sigma_n^2(t_w)$ and

$$G_L(\lambda) = \prod_{n=1}^{\infty} e^{-\frac{2\lambda|c_n(0)|^2(1-e^{-\nu k_n^2\Delta t})^2 e^{-2\nu k_n^2 t_w}}{1+\lambda w_{\infty}^2 a_n(\Delta t, t_w)}}, \quad (71)$$

with the coefficients a_n defined in equation (29). This is the two-times generalization of the result in [23], including arbitrary initial conditions. The averaged two-times roughness follows from G_L as $\langle w^2 \rangle(\Delta t, t_w) = -\partial_{\lambda} G_L(\lambda, t, t_w)|_{\lambda=0}$, which allows to recover the result in equation (28) for the initial condition $|c_n(0)|^2 = T_0/(L\gamma\nu k_n^2)$.

Since the two-times roughness pdf is given by

$$P_L(w^2) = \int_{-i\infty}^{i\infty} \frac{d\lambda}{2\pi i} e^{\lambda w^2} G_L(\lambda, t, t_w), \quad (72)$$

we can extract its scaling properties from the ones of $G_L(\lambda)$ in equation (71). Using $y = \lambda w_{\infty}^2$ and $2|c_n(0)|^2/w_{\infty}^2 = 6w_0^2/(\pi^2 n^2 w_{\infty}^2) = 6/(\pi^2 n^2) s_0^2$ we find

$$w_{\infty}^2 P_L(w^2) = \Phi\left(\frac{w^2}{w_{\infty}^2}; \frac{\Delta t}{t_L}, \frac{t_w}{t_L}, s_0^2\right), \quad (73)$$

$$\Phi\left(x; \frac{\Delta t}{t_L}, \frac{t_w}{t_L}, s_0^2\right) = \int_{-i\infty}^{i\infty} \frac{dy}{2\pi i} e^{yx} \prod_{n=1}^{\infty} \frac{e^{-\frac{y s_0^2 b_n(\frac{\Delta t}{t_L}, \frac{t_w}{t_L})}{1+y a_n(\frac{\Delta t}{t_L}, \frac{t_w}{t_L})}}}{1+y a_n\left(\frac{\Delta t}{t_L}, \frac{t_w}{t_L}\right)} \quad (74)$$

with the coefficients a_n and b_n defined in equations (29) and (30). For a flat initial condition, $T_0 = 0$ and $s_0^2 = w_0^2/w_{\infty}^2 = T_0/T = 0$. With a very similar calculation to the one explained in [23] for the stationary case, we rewrite the function Φ as

$$\Phi\left(x; \frac{\Delta t}{t_L}, \frac{t_w}{t_L}, 0\right) = \sum_{n=1}^{\infty} \frac{e^{-x/a_n}}{a_n} \prod_{m=1, m \neq n}^{\infty} \frac{a_n}{a_n - a_m}, \quad (75)$$

which is essentially the same result in [23] but with two-times dependent coefficients $a_n(\Delta t/t_L, t_w/t_L)$.

By using now a different independent variable, $x' = w^2/\langle w^2 \rangle$, one has

$$\langle w^2 \rangle P_L(w^2) = \Phi' \left(\frac{w^2}{\langle w^2 \rangle}; \frac{\Delta t}{t_L}, \frac{t_w}{t_L}, s_0^2 \right), \quad (76)$$

$$\Phi' \left(x'; \frac{\Delta t}{t_L}, \frac{t_w}{t_L}, s_0^2 \right) \int_{-i\infty}^{i\infty} \frac{dy'}{2\pi i} e^{y'x'} \prod_{n=1}^{\infty} \frac{e^{-\frac{y' s_0^2 b'_n \left(\frac{\Delta t}{t_L}, \frac{t_w}{t_L} \right)}{1+y'a'_n \left(\frac{\Delta t}{t_L}, \frac{t_w}{t_L} \right)}}}{1+y'a'_n \left(\frac{\Delta t}{t_L}, \frac{t_w}{t_L} \right)} \quad (77)$$

and

$$a'_n = \frac{a_n}{\sum_{n=1}^{\infty} a_n + s_0^2 \sum_{n=1}^{\infty} b_n}, \quad b'_n = \frac{b_n}{\sum_{n=1}^{\infty} a_n + s_0^2 \sum_{n=1}^{\infty} b_n}. \quad (78)$$

Equations (73) and (74) are the generalization of equation (15) in [23] that takes into account the aging regime. Equation (76) is a rewriting of the latter using the more convenient normalized variable $w^2/\langle w^2 \rangle$. The parameters are, in both cases, $\Delta t/t_L$, t_w/t_L and s_0^2 . In the *growth and aging* regime in which $\Delta t/t_w$ is finite and the two parameters are very small, *i.e.* $\Delta t/t_L, t_w/t_L \ll 1$, one formally has

$$\frac{\Delta t}{t_w} = \epsilon, \quad \tilde{w}^2 = \mathcal{G}(\epsilon), \quad \langle w^2 \rangle = t_w^{1/2} \mathcal{G}(\epsilon). \quad (79)$$

We can now easily exchange $\Delta t/t_L$ and t_w/t_L by the more convenient set \tilde{w}^2 and $\langle w^2 \rangle/w_\infty^2$. First, we exchange $\Delta t/t_L$ and t_w/t_L by $\Delta t/t_w$ and t_w/t_L . Second, on the one hand $\Delta t/t_w$ is an exclusive function of \tilde{w}^2 . On the other hand, using the results in Sect. 4.3 one can show that

$$\frac{t_w}{t_L} = \left(\frac{\langle w^2 \rangle c_0(T, T_0)}{\tilde{w}^2 w_\infty^2} \right)^2. \quad (80)$$

The factor \tilde{w}^2 enters the last equation, but we can ignore it by redefining the scaling function. We used the EW exponents but this relation can be easily rewritten for generic β , z and ζ . We thus have

$$\langle w^2 \rangle P_L(w^2) = \Phi'' \left(\frac{w^2}{\langle w^2 \rangle}; \frac{\langle w^2 \rangle}{w_\infty^2}, \tilde{w}^2, T, T_0 \right) \quad (81)$$

as proposed in [9] for the generic disordered case.

Let us list and illustrate in some plots different trends in the scaling function Φ evaluated for the flat initial condition. In the numerical evaluations we approximate the infinite sums and products, as in (75), by finite sums and products with different cut-off values, M_1 and M_2 respectively. The main panel in Fig. 14 (a) shows the time-delay evolution of the scaling function Φ for $t_w = 0$ and fixed system size. This corresponds essentially to the results obtained in [23], and shows how the pdf is broader for increasing Δt until the saturation regime is reached. The inset shows the system size dependence, indicating that at fixed t_w the function Φ , tends to a delta-function in the infinite size limit. In Fig. 14 (b) one observes how the pdf is spread at fixed L and Δt while increasing the waiting-time. These results correspond to a flat initial condition $T_0 = 0$.

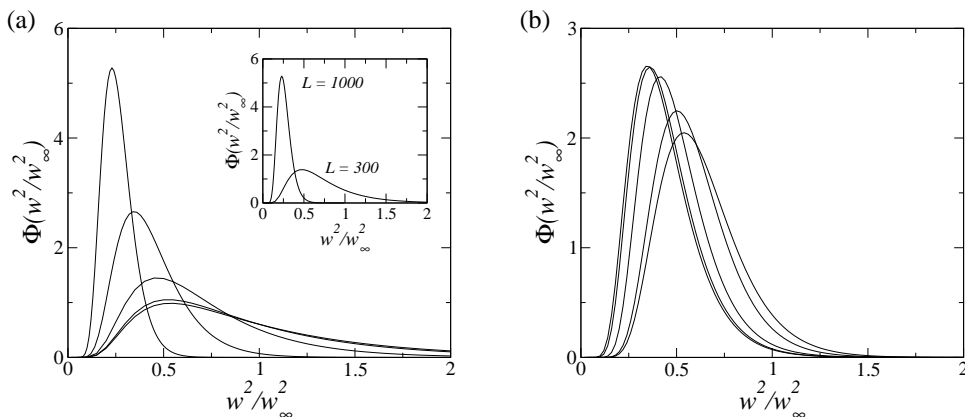


Figure 14. Scaling function $\Phi(w^2/w_\infty^2, \Delta t/t_L, t_w/t_L, 0)$ evaluated with $M_1 = 20$ and $M_2 = 40$. (a) $L = 1000$, $t_w = 0$, and $\Delta t = 10^3, 3 \cdot 10^3, 10^4, 3 \cdot 10^4$, and 10^5 (from left to right). The inset shows a comparison between Φ for different system sizes, $L = 1000$ and $L = 300$ as indicated, at the same waiting-time $t_w = 10^3$ (b) $L = 1000$, $\Delta t = 3 \cdot 10^3$ and $t_w = 1, 10, 10^2, 10^3$, and 10^4 from left to right.

Since it is hard to compute the scaling function Φ for a $T_0 > 0$ initial condition we just present the skewness and kurtosis,

$$\sigma = \frac{\mu_3}{\mu_2^{3/2}}, \quad \kappa = \frac{\mu_4}{\mu_2^2} - 3, \quad (82)$$

respectively, with the centered moments defined as $\mu_2 = \langle w^4 \rangle - \langle w^2 \rangle^2$, $\mu_3 = \langle w^6 \rangle - 3\langle w^4 \rangle \langle w^2 \rangle + 2\langle w^2 \rangle^3$, and $\mu_4 = \langle w^8 \rangle - 4\langle w^6 \rangle \langle w^2 \rangle + 6\langle w^4 \rangle \langle w^2 \rangle^2 - 3\langle w^2 \rangle^4$. The moments of the roughness pdf are given by $\langle (w^2)^m \rangle = (-1)^m \partial_{\lambda^m} G_L(\lambda)|_{\lambda=0}$; then after some algebra one finds

$$\sigma = \frac{\sum_{n=1}^{\infty} [2a_n^3 + 6s_0^2 a_n^2 b_n]}{[\sum_{n=1}^{\infty} (a_n^2 + 2s_0^2 a_n b_n)]^{3/2}}, \quad \kappa = \frac{\sum_{n=1}^{\infty} [6a_n^4 + 24s_0^2 a_n^3 b_n]}{[\sum_{n=1}^{\infty} (a_n^2 + 2s_0^2 a_n b_n)]^2}. \quad (83)$$

Figure 15 displays the time-delay evolution of the skewness and kurtosis for the cases $T > T_0 = 0$ [Fig. 15 (a)] and $T < T_0$ [Fig. 15 (b)]. One can observe that the pdfs are broader and more asymmetric until saturation. Generally, both σ and κ age with a similar Δt and t_w dependencies as the correlation length l or the averaged roughness $\langle w^2 \rangle$. The peculiarities are that the asymptotes corresponding to the infinite size limits grow as $\Delta t^{1/4}$ for the skewness and $\Delta t^{1/2}$ for the kurtosis. The approach to saturation is non-monotonic, showing a bump around $\Delta t \approx t_x(t_w)$. Finally, Fig. 16 shows the T_0 -dependence of the skewness for $t_w = 10^3 \ll t_L$ (the kurtosis behaves in a similar way).

8.2. Center-of-mass displacement distribution

In Sect. 5 we showed that the line's center-of-mass undergoes Brownian motion with mean $\bar{x}(0)$ and variance $\langle D \rangle(\Delta t) = 2T/(\gamma L)\Delta t$. Thus, the center of mass position is

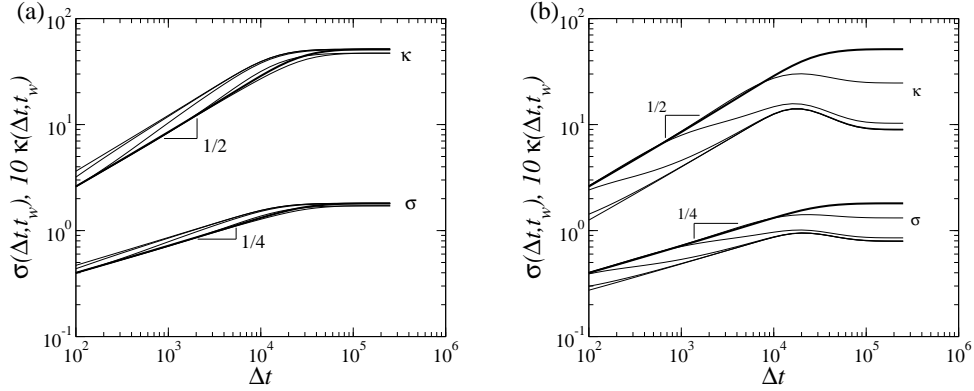


Figure 15. Two-times skewness $\sigma(\Delta t, t_w)$ and kurtosis $\kappa(\Delta t, t_w)$ for the distribution function $P_L(w^2)$ (the kurtosis is rescaled by a factor 10 for clarity). The sums are truncated with $M_3 = 100$. $T = 1$, $L = 1000$, and $t_w = 1, 10, 10^2, 10^3, 10^4$, and 10^5 as indicated. Different initial conditions correspond to (a) $T_0 = 0$ and (b) $T_0 = 5$. The thick lines correspond to the $t_w \rightarrow \infty$ limit.

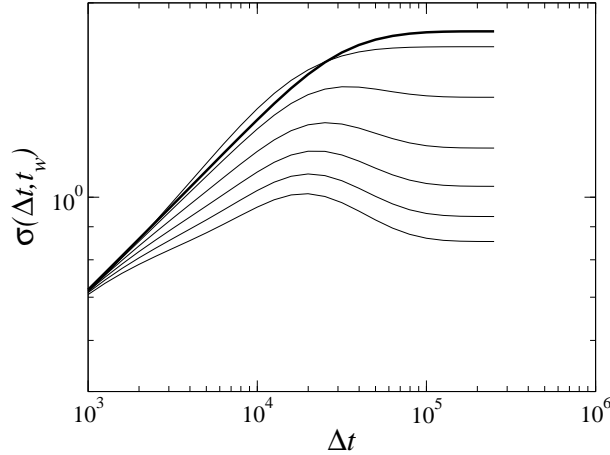


Figure 16. Two-times skewness $\sigma(\Delta t, t_w)$ for the distribution function $P_L(w^2)$. The sums are truncated with $M_3 = 100$. $T = 1$, $L = 1000$, and $T_0 = 0, 1, 2, 3, 4$, and 5 from top to bottom. The waiting-time is $t_w = 10^3$. For comparison, the $t_w = 10^5$ curve, which is the same for all initial temperatures is also included as a thick line.

Gaussian distributed and, after a change of variables, the distribution of the mean-squared-displacement of the center-of-mass is

$$P_L(D) = \frac{e^{-D/(2\langle D \rangle)}}{\sqrt{2\pi\langle D \rangle D}} = \sqrt{\frac{\gamma L}{4\pi T \Delta t D}} \exp\left(-\frac{\gamma L}{4T \Delta t} D\right) \quad (84)$$

which can also be written in the scaled form

$$\langle D \rangle P_L(D) = \Omega\left(\frac{D}{\langle D \rangle}\right), \quad \text{with} \quad \Omega(x) = \frac{e^{-\frac{x}{2}}}{\sqrt{2\pi x}}. \quad (85)$$

8.3. Mean-squared displacement distribution

The mean-squared-displacement satisfies $B(\Delta t, t_w) = w^2(\Delta t, t_w) + D(\Delta t)$. w^2 and D are independent variables (note that the roughness is independent of the zero mode), then the probability function for B can be formally obtained from the inverse Laplace transform of the product of Laplace transforms,

$$P_L(B) = \int_{-\infty}^{\infty} \frac{d\lambda}{2\pi i} e^{\lambda B} K_L(\lambda, \Delta t, t_w), \quad (86)$$

where $K_L = G_L J_L$ is the Laplace transform of $P_L(B)$, $G_L(\lambda, \Delta t, t_w)$ is given by equation (71), and $J_L(\lambda, \Delta t)$ is the Laplace transform of $P_L(D)$,

$$J_L(\lambda, \Delta t) = \frac{1}{\sqrt{2\langle D \rangle \lambda + 1}} = \sqrt{\frac{\gamma L}{4T\Delta t \lambda + \gamma L}}. \quad (87)$$

Then one finds that

$$K_L(\lambda, \Delta t, t_w) = \frac{1}{\sqrt{2[\langle B \rangle - \langle w^2 \rangle] \lambda + 1}} \prod_{n=1}^{\infty} \frac{e^{-\frac{2\lambda |c_n(0)|^2 (1 - e^{-\nu k_n^2 \Delta t})^2 e^{-2\nu k_n^2 t_w}}{1 + \lambda w_{\infty}^2 a_n(\Delta t, t_w)}}}{1 + \lambda w_{\infty}^2 a_n(\Delta t, t_w)}. \quad (88)$$

We now define $y'' = \lambda \langle B \rangle$, $\lambda w_{\infty}^2 a_n(\Delta t, t_w) = y'' a_n''(\Delta t, t_w)$, and

$$a_n''\left(\frac{\Delta t}{t_L}, \frac{t_w}{t_L}\right) = \frac{a_n}{\langle B \rangle / w_{\infty}^2}, \quad b_n''\left(\frac{\Delta t}{t_L}, \frac{t_w}{t_L}\right) = \frac{b_n}{\langle B \rangle / w_{\infty}^2}, \quad (89)$$

and we obtain

$$\langle B \rangle P_L(B) = \Psi\left(\frac{B}{\langle B \rangle}; \frac{\Delta t}{t_L}, \frac{t_w}{t_L}, s_0^2\right). \quad (90)$$

The scaling function is given by

$$\Psi\left(x''; \frac{\Delta t}{t_L}, \frac{t_w}{t_L}, s_0^2\right) = \int_{-i\infty}^{+i\infty} \frac{dy''}{2\pi i} e^{y'' x''} \prod_{n=1}^{\infty} \frac{1}{\sqrt{1 + 2c_n'' y''}} \frac{e^{-\frac{y'' s_0^2 b_n''(\Delta t, t_w)}{1 + y'' a_n''(\Delta t, t_w)}}}{1 + y'' a_n''(\Delta t, t_w)}, \quad (91)$$

with

$$c_n''\left(\frac{\Delta t}{t_L}, \frac{t_w}{t_L}\right) = \frac{\langle D \rangle}{\langle B \rangle}. \quad (92)$$

The pdf of the mean-squared-displacement B can also be written in a scaling form similar to the one found for the roughness.

8.4. The incoherent scattering function

In order to obtain the pdf of the incoherent scattering function we need to use the moment-expansion:

$$p(z) = \int \frac{du}{2\pi} e^{izu} p(u) \quad (93)$$

with

$$p(u) = \sum_{p=0}^{\infty} \frac{u^p}{p!} \left. \frac{\partial^p p(u)}{\partial u^p} \right|_{u=0} = \sum_{p=0}^{\infty} \frac{(-iu)^p}{p!} \langle z^p \rangle. \quad (94)$$

This expression assumes that the series converges and the moments exist. The moments of C_q are

$$\langle C_q^p \rangle = L^{-p} \int dz_1 \dots dz_p e^{-\frac{q^2}{2} \sum_{r,r'=1}^p \langle H \rangle (z_r - z_{r'}; t, t_w)}, \quad (95)$$

where the function

$$\begin{aligned} \langle H \rangle (z; t, t_w) &= \frac{2}{L} \sum_{n=1}^{\infty} \langle S_n \rangle (\Delta t, t_w) e^{ik_n z} \\ &= L^{-1} \int_0^L dz' \langle [\delta x(z', t) - \delta x(z', t_w)] [\delta x(z' - z, t) - \delta x(z' - z, t_w)] \rangle \end{aligned} \quad (96)$$

is the two-times generalization of the height-height correlation function [28].

Using the fact that $\langle H \rangle (0; t, t_w) = \langle w^2 \rangle (\Delta t, t_w)$ and equation (48), one can show that $\langle C_q^p \rangle = \langle C_q \rangle^p I_p$, where the q -dependent function $I_p(t, t_w)$ is given by

$$I_p(\Delta t, t_w, q^2 L) = L^{-p} \int dz_1 \dots dz_p e^{-\frac{q^2}{2} \sum_{r,r'=1; r \neq r'}^p \langle H \rangle (z_r - z_{r'}; \Delta t, t_w)}. \quad (97)$$

From the moment-expansion, using $u' = u(C_q)$, the fact that Tq^2L is a function of $\langle C_q^\infty \rangle$ and calling $T_0 q^2 L = \langle C_q^0 \rangle$, one can write the pdf of the incoherent scattering function in the scaled form

$$\langle C_q \rangle P(C_q) = \Theta \left(\frac{C_q}{\langle C_q \rangle}; \frac{\Delta t}{t_L}, \frac{t_w}{t_L}, C_q^\infty, C_q^0 \right), \quad (98)$$

with

$$\Theta \left(x; \frac{\Delta t}{t_L}, \frac{t_w}{t_L}, C_q^\infty, C_q^0 \right) = \sum_{p=0}^{\infty} \frac{(-i)^p}{p!} \int \frac{du'}{2\pi} e^{iu'x} u'^p I_p \left(\frac{\Delta t}{t_L}, \frac{t_w}{t_L}, q^2 L \right). \quad (99)$$

Although in the last expression the functional form of $\Theta(x)$ is not evident, the scaling properties are clear.

8.5. Fluctuations of the response functions

In quadratic models as the EW elastic line the response functions do not fluctuate. This can be easily shown as follows. Take the roughness integrated linear response (53) without the thermal average. Replacing $c_n^h(t)$ and $c_n(t)$ by their functional form, and using the fact that the two copies evolve with the same thermal noise, one has

$$\chi^{w^2}(t, t_w) = 2L \sum_{n=1}^{\infty} s_n^2 e^{-\nu k_n^2 (t-t_w)}. \quad (100)$$

This result depends on the random fields s_n but it is independent of the thermal noise. For *fixed* random fields this quantity does not fluctuate and the pdf of χ^{w^2} is a delta function. Similarly, one can prove that the displacement and center-of-mass responses are delta-distributed. The same ‘trivial’ result was found for the ferromagnetic coarsening in the $O(N)$ model with $N \rightarrow \infty$ [27].

9. Summary and conclusions

We studied the averaged and fluctuating dynamics of the Edwards-Wilkinson elastic line in one transverse dimension.

Firstly, we analyzed the evolution of correlation functions in terms of the different time scales involved in the problem: the total time, t , the waiting time, t_w , and the saturation time t_L . In particular, for the two-times roughness we found $\langle w^2 \rangle \sim \mathcal{F}_{w^2}[\Delta t/t_w, t_w/t_L, TL, T_0L] \sim \mathcal{F}_{w^2}[t/t_w, t_w/t_L, TL, T_0L]$ (the scaling function in the third member is not identical to the one in the second member but we use the same name to simplify the notation). As mentioned earlier, the problem can also be analyzed in terms of associated length scales obtained from the growing correlation length $\ell(t) = 4\pi^2\nu t^{1/2}$. Then, the relevant length scales are $\ell(t)$, $\ell(t_w)$, and $\ell(t_L) \sim L$. This is reflected for instance in the scaling form of the structure factor in the asymptotic time-delay limit (16), using $k_w \sim \ell(t_w)^{-1}$. The scaling form of the two-times averaged roughness that describes the aging, saturation and equilibrium regimes can be written as

$$\langle w^2 \rangle(\Delta t, t_w) \sim \mathcal{F}_{w^2} \left[\frac{\ell(t)}{\ell(t_w)}, \frac{\ell(t_w)}{\ell(t_L)}, TL, T_0L \right] \quad (101)$$

with $\ell(t) = 4\pi^2\nu t^{1/2}$ and $t_L = L^2/(4\pi^2\nu)$ in the 1 + 1 EW case. This form extends the proposal in (26) to include another scaling variable and thus describe the dynamics of finite lines. It then generalizes the celebrated Family-Vicsek scaling [29] to include the preasymptotic non-equilibrium regime. The aging regime corresponds to $\ell(t_w) \ll \ell(t_L)$ and the function $\mathcal{F}_{w^2}[\ell(t)/\ell(t_w), 0, T_0L, TL] \sim \ell^\zeta \mathcal{F}[\ell(t)/\ell(t_w)]$, leading to (26) with all the temperature dependent asymptotic properties already detailed in the central part of the manuscript. The saturation regime is reached by taking $t \gg t_L$ at fixed t_w ; this means $\ell(t_w)/\ell(t) \ll 1$ and $\ell(t)/\ell(t_L) \gg 1$. Finally, the usual stationary equilibrium regime corresponds to $t_w \gg t_L$, and for a power-law growth one recovers the Family-Vicsek scaling $\langle w^2 \rangle \sim L^\zeta \mathcal{F}_{w^2}[\ell(\Delta t)/L]$.

We also showed that the two-times dependent correlation length defined through the dynamics of the structure factor, satisfies a similar scaling law

$$l(t, t_w) \sim \mathcal{F}_l \left[\frac{\ell(t)}{\ell(t_w)}, \frac{\ell(t_w)}{\ell(t_L)}, \frac{T}{T_0} \right]. \quad (102)$$

Note that although this expression gives the full aging behaviour of $l(t, t_w)$, it can be completely rationalized using the simple length scale $\ell(t)$. For instance, in the aging regime, one finds that regions with $\ell(t) \sim \ell(t_w)$ are equilibrated at the working temperature, while regions with $\ell(t) > \ell(t_w)$ are still not at equilibrium.

Interestingly enough, we demonstrated that ordering or disordering non-equilibrium dynamics following a quench from higher temperature or a heating process from a lower temperature are characterized by a higher or lower effective temperature than the one of the bath. This result is consistent with the intuitive interpretation of the effective temperature with higher (lower) values associated to more (less) disordered

configurations than the equilibrium ones at the working temperature. A similar dependence on the initial condition was derived by Berthier *et al* in the $2d$ XY model [25].

The two-times length scale l also shows the latter property. In the aging regime, for fixed t_w the length grows with Δt for all $T \neq T_0$ while for fixed Δt it grows with t_w when $T_0 > T$ and it decreases with t_w when $T_0 < T$. The former behaviour is similar to what is observed in conventional glassy systems such as the $3d$ Edwards-Anderson spin glass [19] and models of particles in interaction [18]. The heating procedure was not studied in such cases.

The wave-vector dependent correlation $\langle C_q \rangle$ that plays the role of the incoherent scattering function in studies of glassy systems is particularly interesting. We showed that, although $\langle C_q \rangle$ is simply related to the roughness, the characteristic multiplicative scaling is not easily detected in $\langle C_q \rangle$. This might be the case in other systems, such as colloidal glasses where it was recently shown that diffusive correlations clearly display multiplicative aging scaling [34], while this was not previously reckoned in the study of the incoherent scattering function [17].

One can also observe that the aging behaviour of $\langle C_q \rangle$ resembles strongly the experimental results in laponite [17]. In particular it was found in this system that the incoherent scattering function displays a waiting-time dependent plateau at long time-delay. This suggests that a similar equilibration mechanism might be at work in the relaxation dynamics of the rather complex laponite samples, where some competing length scale is confining the particle fluctuations, thus leading to saturation of the incoherent scattering function. The waiting-time dependent saturation is in line with the fact that effective temperatures, measured through the FDT, should become the bath temperature at fixed time-delay and sufficiently long waiting times where saturation is found. The measurements in [30] are such that the effective temperature does indeed tend to the bath temperature at fixed working frequency – equivalently time-delay – when t_w is large enough, although this result remains controversial [35].

With this analytic study we showed that the qualitative aging dynamics of the vortex glass [10, 11] as well as the elastic line in a quenched disordered environment [8, 9] is mainly due to the non-equilibrium relaxation of the pure elastic lines. The effect of quenched disorder and line-line interactions is to change the details of the scaling, more precisely the temperature and time-dependence in $\ell(t)$, but not the qualitative features. Along this line, the study of the aging dynamics of the pure KPZ equation [36] will allow one to better rationalize the results in [14], where the aging dynamics of this equation with a disordered potential – and driving force – was analyzed. Furthermore, the results obtained here could be strongly related to the non-equilibrium relaxation dynamics of confined polymers [37].

We presented the first analytic calculation of finite-size fluctuations during an out-of-equilibrium relaxation. This study complements the analysis in [33] and [23] for the width fluctuations at saturation and growth and in [31, 32] for other quantities such as the maximum height displacement – indeed, it is also simple to include the t_w -dependence in this calculation. Our results make explicit the dependence on the

waiting-time and display the crossover to equilibrium. They constitute a benchmark for Rácz proposal to classify interface dynamics into universality classes [20], now extending it to the non-equilibrium relaxation.

As regards the time-reparametrization invariance scenario for glassy dynamics we do not expect it to hold, without modification, in models with multiplicative aging scaling. Following the steps sketched in [22] to study the asymptotic averaged dynamics of the EW line (or massless scalar field) and its corresponding dynamic action, one soon realizes that the multiplicative $t_w^{1/2}$ factor has to be extracted from the asymptotic analysis to search for time-reparametrization invariance. This is similar to what was shown in [27] for the $O(N)$ model in the large N limit. One should also notice that the dynamics of the EW line depends on the dimensionality of the transverse space. For instance, one can show that for infinite systems diffusion disappears and the aging regime persists at infinite waiting-times (*i.e.* the scaling becomes additive) in two transverse dimensions [24]. One has then the interesting possibility of testing the time-reparametrization invariance scenario in the ‘critical’ EW equation with two transverse dimensions. The detailed analysis of the dynamic symmetries of the generic EW line goes beyond the scope of this article.

We conclude with a note on the relevance of our results for coarsening phenomena. The domain walls between equilibrated regions during domain growth are usually described as elastic objects. Recently, the distribution of domain sizes and perimeter lengths in two-dimensional Ising ferromagnetic growth was shown to be unexpectedly non-trivial [38]. The wide distribution of domain sizes and domain wall lengths combined with the highly non-trivial fluctuating dynamics of finite-length elastic lines derived here suggest that characterising the fluctuations of standard two-times observables in domain-growth phenomena can be a quite complicated problem.

Acknowledgments

We thank the Universidad Nacional de Mar del Plata, Argentina, for hospitality during the preparation of this work and C. Chamon, D. Domínguez, T. Giamarchi, G. Schehr and H. Yoshino for very useful discussions. LFC acknowledges financial support from Secyt-ECOS P. A01E01 and PICS 3172, SB from the Swiss National Science Foundation under MaNEP and Division II, and JLI from CONCIET PIP05-5648 and ANPCYT PICT04-20075. LFC is a member of Institut Universitaire de France.

- [1] Barabási A-L and Stanley HE, 1995 *Fractal concepts in surface growth* (Cambridge: Cambridge University Press)
- Halpin-Healey T and Zhang Y-C, 1995 *Phys. Rep.* **254** 215
- [2] Bray AJ, 1994 *Adv. Phys.* **43** 357

- [3] Blatter G, Feigel'man MV, Geshkenbein VB, Larkin AI and Vinokur VM, 1994 *Rev. Mod. Phys.* **66** 1125
Nattermann T and Scheidl S, 2000 *Adv. Phys.* **49** 607
- [4] Hansen A, Hinrichsen EL and Roux S, 1991 *Phys. Rev. Lett.* **66** 2476
Bouchaud E, 1997 *J. Phys.: Condens. Matter* **9** 4319
Alava M, Nukalaz PKVV and Zapperi S, 2006 *Adv. Phys.* **55** 349
- [5] Sahimi M, 1995 *Flow and Transport in Porous Media and Fractured Rock* (New York: John Wiley & Sons)
Alava M, Dubé M and Rost M, 2004 *Adv. Phys.* **53** 83
- [6] Edwards SF and Wilkinson DR, 1982 *Proc. R. Soc. London, Ser. A* **381** 17
- [7] Cugliandolo LF, 2004 *Slow Relaxations and Nonequilibrium Dynamics in Condensed Matter (Les Houches-Ecole d'Ete de Physique Theorique vol 77)*, ed J-L Barrat *et al.* (Berlin: Springer) Also available as [cond-mat/0210312]
- [8] Yoshino H, 1996 *J. Phys. A: Math. Gen.* **29** 1421
Yoshino H, 1998 *Phys. Rev. Lett.* **81** 1493
Barrat A, 1997 *Phys. Rev. E* **55** 5651
- [9] Bustingorry S, Iguain JL, Chamon S, Cugliandolo LF and Domínguez D, 2006 *Europhys. Lett.* **76** 856
- [10] Bustingorry S, Cugliandolo LF and Domínguez D, 2006 *Phys. Rev. Lett.* **96** 027001
Bustingorry S, Cugliandolo LF and Domínguez D, 2007 *Phys. Rev. B* **75** 024506
- [11] Schehr G and Rieger H, 2005 *Phys. Rev. B* **71** 184202
Schehr G and Le Doussal P, 2005 *Europhys. Lett.* **71** 290
- [12] Portier F, Kriza G, Sas B, Kiss LF, Pethes I, Vad K, Keszei B and Williams FIB, 2002 *Phys. Rev. B* **66** 140511
Exartier R and Cugliandolo LF, 2002 *Phys. Rev. B* **66**, 012517
Du X, Li G, Andrei EY, Greenblatt M and Shuk P, 2007 *Nature Phys.* **3**, 111
- [13] Kolton A, Rosso A and Giamarchi T, 2005 *Phys. Rev. Lett.* **95** 180604
- [14] Ramasco JJ, Lopez JM and Rodriguez MA, 2006 *Europhys. Lett.* **76** 554
- [15] Kardar M, Parisi G and Zhang YC, 1986 *Phys. Rev. Lett.* **56** 889
- [16] Cugliandolo LF and Le Doussal P, 1996 *Phys. Rev. E* **53** 1525
Cugliandolo LF, Kurchan J and Le Doussal P, 1996 *Phys. Rev. Lett.* **76** 2390
Konkoli Z, Hertz J and Franz S, 2001 *Phys. Rev. E* **64** 051910
Konkoli Z and Hertz J, 2003 *Phys. Rev. E* **67** 051915
Goldschmidt YY, 2006 *Phys. Rev. E* **74** 021804
- [17] Bonn D, Tanaka H, Wegdam G, Kellay H and Meunier J, 1999 *Europhys. Lett.* **45** 52
Tanaka H, Jabbari-Farouji S, Meunier J and Bonn D, 2005 *Phys. Rev. E* **71** 021402
- [18] Parisi G, 1999 *J. Phys. Chem.* **103**, 4128
Parsaeian A and Castillo HE, 2007 *Nature Phys.* **3** 26
- [19] Jaubert LDC, Chamon C, Cugliandolo LF and Picco M, 2007 *J. Stat. Mech.* P05001
- [20] Rácz Z, 2003 *SPIE Proceedings* **5112** 248
- [21] Chamon C, Kennett MP, Castillo HE and Cugliandolo LF, 2002 *Phys. Rev. Lett.* **89** 217201
Castillo HE, Chamon C, Cugliandolo LF and Kennett MP, 2002 *Phys. Rev. Lett.* **88** 237201
Castillo HE, Chamon C, Cugliandolo LF, Iguain JL and Kennett MP, 2003 *Phys. Rev. B* **68** 134442
Chamon C, Charbonneau P, Cugliandolo LF, Reichman D and Sellitto M, 2004 *J. Chem. Phys.* **121** 10120
- [22] Chamon C and Cugliandolo LF, 2007 Fluctuations in glassy systems *Preprint* arXiv:0704.0684.
- [23] Antal T and Rácz Z, 1996 *Phys. Rev. E* **54** 2256
- [24] Cugliandolo LF, Kurchan J and Parisi G, 1994 *J. Phys. I* **4** 1641
- [25] Berthier L, Holdsworth PWC and Sellitto M, 2001 *J. Phys. A: Math. Gen.* **34** 1805
- [26] Ciuchi S and de Pasquale F, 1988 *Nucl. Phys. B* **300** 31
Cugliandolo LF and Dean DS, 1995 *J. Phys. A: Math. Gen.* **28** L453

- Cugliandolo LF and Dean DS, 1995 *J. Phys. A: Math. Gen.* **28** 4213
- [27] Chamon C, Cugliandolo LF, Yoshino H, 2006 *J. Stat. Mech.* P01006
- [28] Yang H-N, Lu T-M and Wang G-C, 1992 *Phys. Rev. Lett.* **68** 2612
Yang H-N, Lu T-M and Wang G-C, 1993 *Phys. Rev. B* **47** 3911
- [29] Family F and Vicsek T, 1985 *J. Phys. A: Math. Gen.* **18** L75
- [30] Abou B and Gallet F, 2004 *Phys. Rev. Lett.* **93** 160603
- [31] Majumdar SN and Comtet A, 2004 *Phys. Rev. Lett.* **92** 225501
Majumdar SN and Comtet A, 2005 *J. Stat. Phys.* **119** 777
- [32] Schehr G and Majumdar SN, 2006 *Phys. Rev. E* **73** 056103
- [33] Foltin G, Oerding K, Rácz Z, Workman RL and Zia RKP, 1994 *Phys. Rev. E* **50** R639
Plischke M, Rácz Z and Zia RKP, 1994 *Phys. Rev. E* **50** 3589
Rácz Z and Plischke M, 1994 *Phys. Rev. E* **50** 3530
Bramwell ST, Holdsworth PCW and Pinton JF, 1998 *Nature* **396** 552
- [34] Wang P, Song C and Makse HA, 2006 *Nature Phys.* **2** 526
- [35] Greinert N, Wood T and Bartlett P, 2006 *Phys. Rev. Lett.* **97** 265702
Jabbari-Farouji S, Mizuno D, Atakhorrami M, MacKintosh FC, Schmidt CF, Eiser E, Wegdam GH and Bonn D, 2007 *Phys. Rev. Lett.* **98** 108302
- [36] Bustingorry S, in preparation
- [37] Rahmani A, Castelnovo C, Schmit J and Chamon C *Preprint* arXiv:0704.1663
- [38] Arenzon JJ, Bray AJ, Cugliandolo LF and Sicilia A, 2007 *Phys. Rev. Lett.* **98** 145701
Sicilia A, Arenzon JJ, Bray AJ, Cugliandolo LF, in preparation